

Aneuploidy can be an evolutionary diversion on the path to adaptation

Ilia Kohanovski^{a,b,1}, Martin Pontz^{a,1}, Pétra Vande Zande^c, Anna Selmecki^c, Orna
Dahan^d, Yitzhak Pilpel^d, Avihu H. Yona^e, and Yoav Ram^{a,*}

^aSchool of Zoology, Faculty of Life Sciences, Tel Aviv University, Tel Aviv, Israel

^bSchool of Computer Science, Reichman University, Herzliya, Israel

^cDepartment of Microbiology and Immunology, University of Minnesota Medical School, Minneapolis, MN

^dDepartment of Molecular Genetics, Weizmann Institute of Science, Rehovot, Israel

^eInstitute of Biochemistry, Food Science and Nutrition, Robert H. Smith Faculty of Agriculture, Food and
Environment, The Hebrew University of Jerusalem, Israel

¹These authors contributed equally to this work

*Corresponding author: yoav@yoavram.com

January 21, 2024

Classifications. Biological Sciences: Evolution, Genetics, Microbiology, Population Biology.

Keywords: whole-chromosome duplication, evolutionary model, adaptive evolution

Abstract

Aneuploidy is common in eukaryotes, often leading to decreased fitness. However, evidence from fungi and human tumour cells suggests that specific aneuploidies can be beneficial under stressful conditions and facilitate adaptation. In a previous evolutionary experiment with yeast, populations evolving under heat stress became aneuploid, only to later revert to euploidy after beneficial mutations accumulated. It was therefore suggested that aneuploidy is a "stepping stone" on the path to adaptation. Here, we test this hypothesis. We use Bayesian inference to fit an evolutionary model with both aneuploidy and mutation the experimental results. We then predict the genotype frequency dynamics during the experiment, demonstrating that most of the evolved euploid population likely did not descend from aneuploid cells, but rather from the euploid wildtype population. Our model shows how the beneficial mutation supply—the product of population size and beneficial mutation rate—determines the evolutionary dynamics: with low supply, much of the evolved population descends from aneuploid cells; but with high supply, beneficial mutations are generated fast enough to outcompete aneuploidy due to its inherent fitness cost. Our results suggest that despite its potential fitness benefits under stress, aneuploidy can be an evolutionary "diversion" rather than a "stepping stone": it can delay, rather than facilitate, the adaptation of the population, and cells that become aneuploid may leave less descendants compared to cells that remain diploid.

34 Introduction

Aneuploidy is an imbalance in the number of chromosomes in the cell: an incorrect karyotype.
36 Evidence suggests aneuploidy is very common in eukaryotes, e.g. animals^{49,38,2}, and fungi^{41,73,45,62}.
Aneuploidy has been implicated in cancer formation, progression, and drug resistance^{4,51,49,48,23,34}.
38 It is also common in protozoan pathogens of the *Leishmania* genus, a major global health concern³⁶,
and contributes to the emergence of drug resistance⁵² and virulence³⁷ in fungal pathogens, which
40 are under-studied⁴⁷, despite infecting a billion people per year, causing significant morbidity in >150
million and death in >1.5 million people per year^{52,47}.
42 Experiments with human and mouse embryos found that most germ-line aneuploidies are lethal. Ane-
uploidies are also associated with developmental defects and lethality in other multicellular organ-
44 isms⁵⁵. For example, aneuploid mouse embryonic cells grow slower than euploid cells⁶⁷. Similarly,
in unicellular eukaryotes growing in benign conditions, aneuploidy usually leads to slower growth and
46 decreased overall fitness, in part due to proteotoxic stress due to increased expression, gene dosage
imbalance, and hypo-osmotic-like stress^{39,65,41,55,50,27,72,66,68,46}.
48 However, aneuploidy can be beneficial under stressful conditions due to the wide range of phenotypes
it can produce, some of which are advantageous^{41,68}. Indeed, in a survey of 1,011 yeast strains,
50 aneuploidy has been detected in about 19%⁴². Thus, aneuploidy can lead to rapid adaptation in
unicellular eukaryotes^{17,64,21,44}, as well as to rapid growth of somatic tumour cells^{51,57}. For example,
52 aneuploidy in *Saccharomyces cerevisiae* facilitates adaptation to a variety of stressful conditions like
heat and pH⁷⁰, copper^{8,17}, salt^{11,46}, and nutrient limitation^{12,19,1}, with similar results in *Candida*
54 *albicans*⁶⁸. Importantly, aneuploidy can also lead to drug resistance in pathogenic fungi such as
C. albicans^{54,53,16} and *Cryptococcus neoformans*⁵⁸, which cause candidiasis and meningoencephalitis,
56 respectively. Although we focus here on aneuploidy, a similar phenomena of adaptation via gene
duplication or amplification has been observed in yeast³³, bacteria⁶⁰, and DNA viruses¹³.
58 Yona et al.⁷⁰ demonstrated experimentally the importance of aneuploidy in adaptive evolution. They
evolved populations of *S. cerevisiae* under strong heat stress. The populations adapted to the heat stress
60 within 450 generations, and this adaptation was determined to be due a duplication of Chromosome III.
Later on, after more than 1,500 generations, the populations reverted back to an euploid state, while
62 remaining adapted to the heat stress. Aneuploidy was therefore suggested to be a transient adaptive
solution, because it can rapidly appear and take over the population under stressful conditions, and
64 can then be rapidly lost when the cost of aneuploidy outweighs its benefit—after the stress is removed,
or after refined beneficial mutations appear and fixate⁷⁰. Furthermore, it has been suggested that

66 aneuploidy is an evolutionary “stepping stone” that facilitates future adaptation by genetic mutations,
which require more time to evolve^{70,69}.

68 Here, we test the hypothesis that aneuploidy is a an evolutionary stepping stone that facilitates adaptive
evolution by genetic mutations Yona et al.⁶⁹. We develop an evolutionary genetic model and fit it to the
70 experimental results of Yona et al.⁷⁰ to predict the genotype frequency dynamics in the experimental
populations, thereby estimating the frequency of evolved euploid cells that descended from aneuploid
72 cells. Our results show that although aneuploidy reached high frequencies in the experimental
populations, the majority of cells in the evolved euploid population likely did not descend from
74 aneuploid cells, but rather directly from wild-type euploid cells. These suggests that at the lineage
level, aneuploidy may be an “evolutionary diversion”, rather than a stepping stone, on the path to
76 adaptation.

Results

78 In the heat-stress experiment of Yona et al.⁷⁰, four populations of *S. cerevisiae* evolved under 39 °C.
Aneuploidy reached high frequency (>95%) in all four experimental repetitions in the first 450
80 generations. Two of the repetitions, marked *H2* and *H4*, carried no large-scale duplications other
than a Chromosome III trisomy. These two repetitions continued to evolve under the same conditions,
82 wherein aneuploidy was eliminated by generation 1,700 and 2,350 in *H4* and *H2*, respectively.

Evolutionary genetic model. To explore the dynamics during the evolutionary experiments, we
84 developed an evolutionary genetic model, fitted the model to empirical data, and used it to predict the
genotype frequency dynamics, or specifically, the fraction of the evolved euploid population descended
86 from aneuploid cells.

The model includes the effects of natural selection, genetic drift, aneuploidy, and mutation (i.e., other
88 genetic variants), and follows a population of cells characterized by their genotype: euploid wild-
type, $2n$, is the ancestral diploid genotype; euploid mutant, $2n^*$, has a diploid karyotype and a single
90 beneficial mutation; aneuploid wild-type, $2n+1$, has an extra chromosome due to a chromosome
duplication event; and aneuploid mutant, $2n+1^*$, has and extra chromosome (like $2n+1$) and a
92 beneficial mutation (like $2n^*$). Note that ‘mutation’ here refers to point mutations and other genetic
variants unrelated to aneuploidy. Fitness values of the different genotypes are denoted by w_{2n} , w_{2n^*} ,
94 w_{2n+1} , and w_{2n+1^*} , and the rate of mutation and aneuploidy are denoted by μ and δ , respectively. See
Figure 1 for an illustration of the model.

96 We fitted this model to the experimental results⁷⁰—time for fixation (frequency >95%) and for loss
 98 (frequency <5%) of aneuploidy—using approximate Bayesian computation with sequential Monte Carlo
 100 (ABC-SMC)⁵⁹, thereby inferring the model parameters: rates of aneuploidy (i.e., mis-segregation,
 non-disjunction) and mutation and the fitness of all genotypes. We then sampled posterior predictions
 for the genotype frequency dynamics using the estimated parameter values and compared different
 versions of the model to test additional hypotheses about the evolutionary process.

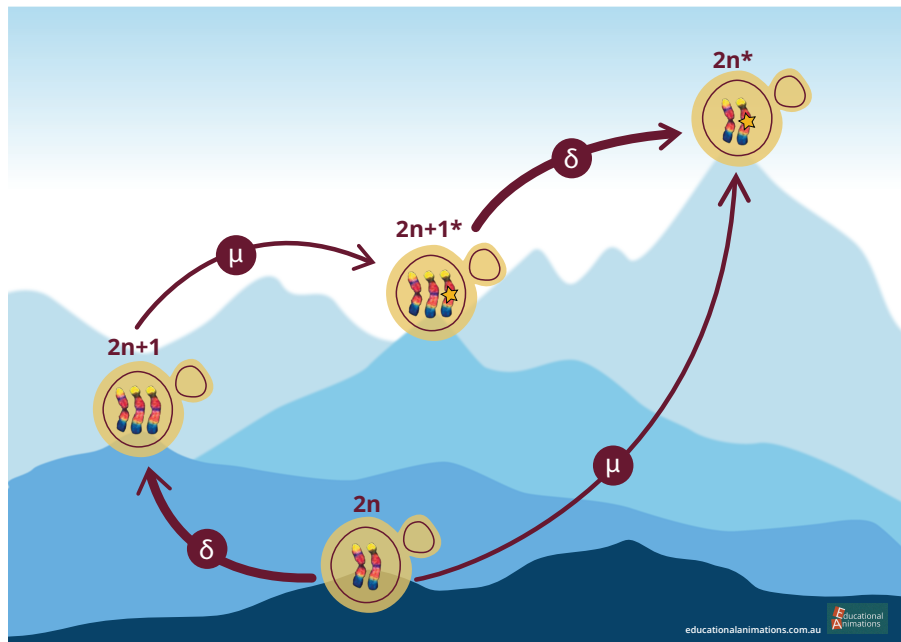


Figure 1: Model Illustration. There are four genotypes in our model: euploid wild-type, $2n$; euploid mutant, $2n^*$; aneuploid wild-type, $2n+1$; and aneuploid mutant, $2n+1^*$. Overall there are two possible trajectories from $2n$ to $2n^*$. Arrows denote transitions between genotypes, with transition rates μ for the beneficial mutation rate and δ for the aneuploidy rate. Elevation differences illustrate the expected, rather than the assumed, fitness differences between the genotypes.

102 **Estimated rates and fitness effects of aneuploidy and mutation.** We inferred the posterior distribution
 104 of model parameters (Figure 2). We report parameter estimates using the MAP (maximum a
 posteriori) and providing the 50% HDI (highest density interval) in square brackets. See Supplementary Material for sensitivity analysis.

106 The estimated beneficial mutation rate is $\mu = 2.965 \cdot 10^{-6}$ [$2.718 \cdot 10^{-7} - 3.589 \cdot 10^{-6}$] per genome
 per generation (that is, roughly 3 out of 10^6 cell divisions produce a mutant cell with a fitness
 108 advantage). From the literature, the mutation rate per base pair is roughly $2 - 3 \cdot 10^{-10}$ (refs.^{74,35}), but
 it may be higher under heat stress, as several stresses²⁰, including heat²², may cause hypermutation
 110 in yeast. If we assume a 10-fold increase over the mutation rate reported in the literature, then the
 estimated beneficial mutation rate can be explained by a genomic target size of 1,000 base pairs

112 (that is, 1,000 base pairs across the genome in which a mutation would provide a fitness advantage):
113 $3 \cdot 10^{-10} \times 10 \times 1,000 = 3 \cdot 10^{-6}$. Supporting this, Jarolim et al.²⁵ found 279 genes that contributed
114 to survival after a sudden shift from 30 °C to 50 °C, and Flynn et al.¹⁴ used a deep mutational
115 scan of a single protein, Hsp90, to find 465 amino-acid variants (out of 14,160) that significantly
116 increased growth rate in 37 °C. Furthermore, Yona et al.⁷⁰ found at least 10 genes on Chromosome
117 III that increased heat tolerance when over-expressed. Assuming that other chromosomes also have
118 a similar number of heat-tolerance genes (and even more, as Chromosome III is one of the smallest
119 chromosomes¹⁸), we get a total of 160 heat-tolerance genes in the genome. Indeed, mutations were
120 found in 97 genes in an evolutionary experiment with yeast under heat stress²². Thus, to get a genomic
121 target size of 1,000, it is enough that the average gene target size (number of base pairs in a gene in
122 which a mutation is beneficial) is 6.25 base pairs. For example, Kohn and Anderson³⁰ found a target
size of 11 in a proton exporter gene (*PMA1*) that contributes to high-salt adaptation.

124 The estimated rate of aneuploidy (i.e., mis-segregation, non-disjunction), $\delta = 1.72 \cdot 10^{-3}$ [$1.47 \cdot 10^{-3} -$
125 $2.786 \cdot 10^{-3}$] is higher than in previous studies: for Chromosome III in diploid *S. cerevisiae*, Zhu
126 et al.⁷⁴ estimated $6.7 \cdot 10^{-6}$ chromosome gain events per generation, and Kumaran et al.³² estimate
127 $3.0 \cdot 10^{-5} - 4.3 \cdot 10^{-5}$ chromosome loss events per generation (95% confidence interval). However,
128 this difference may be partly explained by an increased aneuploidy rate during heat stress: heat shock
can increase the rate of chromosome fragment loss by 2-3 orders of magnitude⁵.

130 The estimated fitness values are $w_{2n+1} = 1.022$ [1.021 – 1.023], $w_{2n+1*} = 1.025$ [1.024 – 1.026],
131 $w_{2n*} = 1.028$ [1.026 – 1.029], all relative to the fitness of $2n$, which is set to $w_{2n} = 1$. If we allow for
132 transitions (mutation, chromosome loss and gain) to less-fit genotypes (e.g., $2n^*$ to $2n+1^*$), then we
infer similar but slightly different values, see Supplementary Material.

134 **Model comparison and goodness-of-fit.** To assess the fit of our model to the data, we use posterior
135 predictive checks, in which we simulate the frequency dynamics using MAP parameter estimates and
136 compare them to the data. Our model fits the data well: $2n^*$ fixed in 63% of simulations by generation
1,700 and in 100% of simulations by generation 2,350 (Figure 3).

138 However, a model without aneuploidy (where the aneuploidy rate is fixed at zero, $\delta = 0$), fails to
139 explain the experimental observations (Figure 3). The estimated mutation rate without aneuploidy is
140 $\mu = 7.98 \cdot 10^{-9}$ [$7.906 \cdot 10^{-9} - 8.138 \cdot 10^{-9}$], much lower compared to a model with aneuploidy. The
141 fitness of the mutant is also much lower at $w_{2n*} = 1.013$ [1.012 – 1.013]. This is because, without
142 aneuploidy, a high mutation rate or fitness effect will lead to faster appearance and fixation of $2n^*$ than
in the experimental observations.

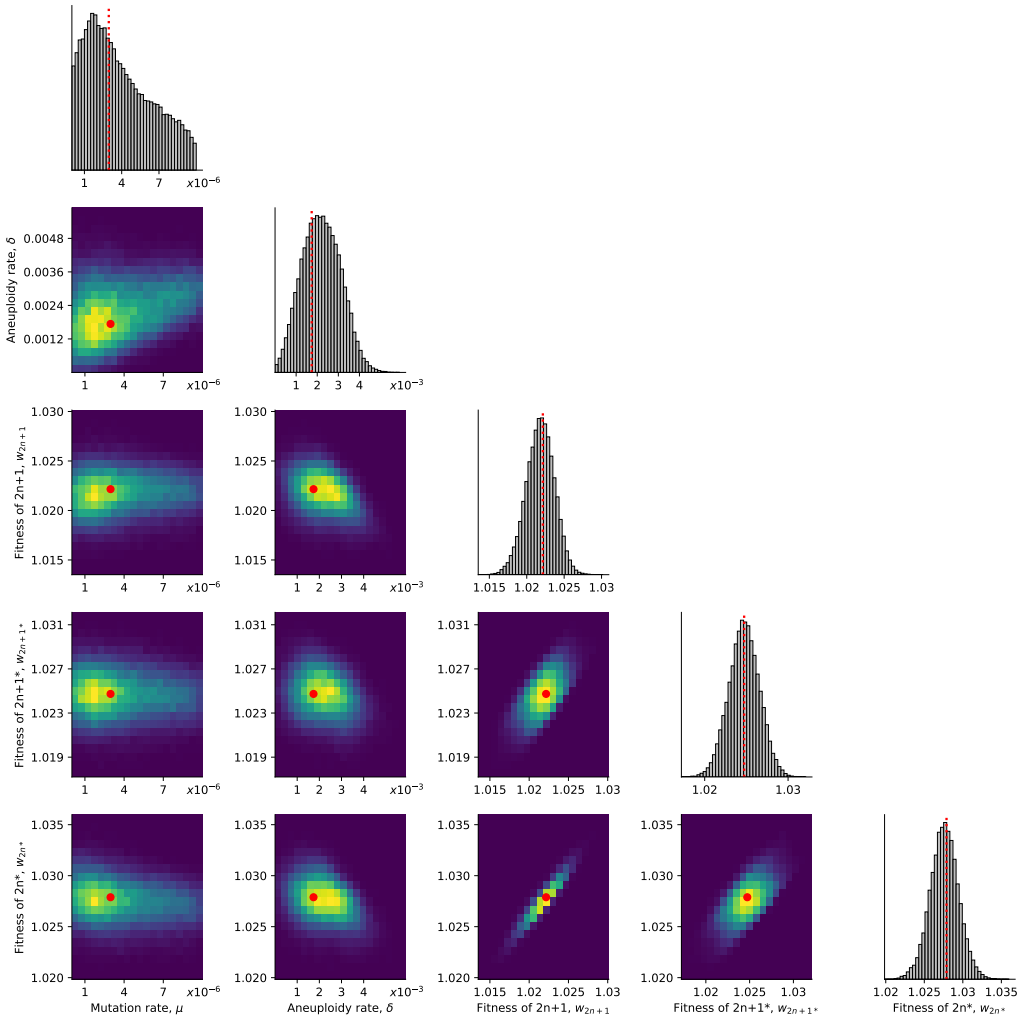


Figure 2: Posterior distribution of model parameters. On the diagonal, the marginal posterior distribution of each model parameter. Below the diagonal, the joint posterior distribution of pairs of model parameters (dark purple and bright yellow for low and high density, respectively). Red markers and orange lines for the joint MAP estimate (which may differ from the marginal MAP, as the marginal distribution integrates over all other parameters).

144 We also checked a model in which aneuploidy occurs but is adaptively neutral compared to the wild-type, that is, $w_{2n+1} = w_{2n}$ and $w_{2n+1^*} = w_{2n^*}$ but $\delta > 0$. This model fits the data better than the model
 146 with no aneuploidy (in which $\delta = 0$), but worse than a model with positive selection for aneuploidy, in which $w_{2n} < w_{2n+1} < w_{2n+1^*} < w_{2n^*}$ (Figure 3).

148 **Model predictions of genotype frequency dynamics.** We simulated 50 replicate genotype frequency dynamics using the MAP estimate parameters. Figure 4A shows the simulated frequencies of
 150 the four genotypes ($2n$, $2n+1$, $2n+1^*$ and $2n^*$), as well as the frequencies of $2n^*$ cells that arose from either $2n+1$ cells via a sequences of mutation and chromosome loss events ($2n_A^*$), or directly from
 152 $2n$ cells via a mutation event ($2n_M^*$). We find that $2n+1^*$ never reaches substantial frequency as it is

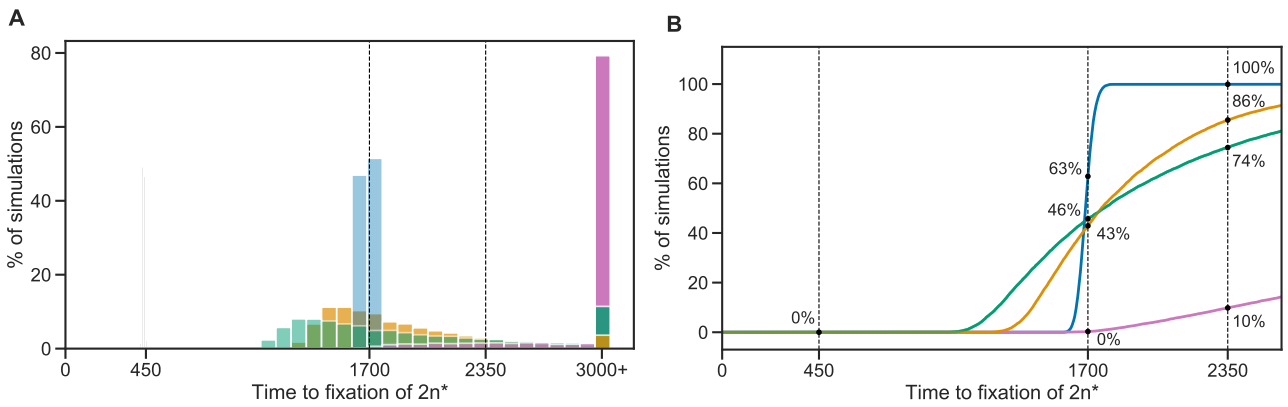


Figure 3: Model fit with and without aneuploidy. The distribution of time to fixation of $2n^*$ (i.e., adaptation time) in 10,000 simulations using MAP parameters of the model with beneficial aneuploidy (blue; $\delta > 0$, $w_{2n} < w_{2n+1} < w_{2n+1}^* < w_{2n}^*$) compared to alternative models: a model with the same parameter values but without aneuploidy (gray, $\delta = 0$, concentrated at $t = 450$); a model fitted to the data assuming no aneuploidy (green, $\delta = 0$); a model fitted to the data assuming neutral aneuploidy (yellow, $\delta > 0$, $w_{2n+1} = w_{2n}$, $w_{2n+1}^* = w_{2n}^*$); and a model with beneficial aneuploidy and an extended prior distribution (pink). In the experiment by Yona et al.⁷⁰, one population lost aneuploidy by generation 1,700 and another by generation 2,350 (dashed lines) but not before generation 450. Thus, the blue distribution has a better fit compared to the other distributions (the gray distribution has a particularly poor fit). The MAP likelihood (eq. (4)) is 0.84, 0.78, 0.67, and 0.14 for the models represented by blue, yellow, green, and pink distributions, respectively. **(A)** Histogram of the time to fixation of $2n^*$. The last bin contains all values equal or greater than 3,000. **(B)** Cumulative distribution of the time to fixation.

quickly replaced by $2n^*$ in a process similar to *stochastic tunneling*^{24,31}.

- 154 To test the hypothesis that aneuploidy facilitates adaptation, we estimated F_A , the expected frequency
 155 of $2n^*$ that arose from $2n+1$, computed as the average frequency of such $2n_A^*$ cells at the end of
 156 simulations using the MAP estimate parameters. Surprisingly, we observe that the majority of $2n^*$
 157 cells are $2n_M^*$, a product of a direct mutation in $2n$ cells, rather than descending from $2n+1$ cells
 158 ($F_A^{MAP} = 0.106$, average end point of 50 purple lines in Figure 4A). This is despite the fact that the
 159 $2n+1$ genotype reaches high frequencies in the population (at least 0.98, Figure 4A).
- 160 This result is not unique to the MAP parameter estimate. We simulated genotype frequency dynamics
 161 using parameter samples from the posterior distribution, and computed the posterior distribution of
 162 F_A (Figure 4B). The posterior mode F_A was just 0.147 [0.0154-0.370 95% CI] and only in 489 of
 163 100,000 posterior samples (0.489%) F_A was larger than 0.5 (see Supporting Material for results when
 164 transitions to less-fit genotypes are allowed, such as $2n^*$ to $2n+1^*$). Thus, if we sample a random

cell from the evolved $2n^*$ population, it is more likely to have descended directly from an euploid
166 cell than from an aneuploid cell. The probability of $2n^*$ descending from $2n+1$ (F_A) increases
with the aneuploidy rate, δ , and decreases with both the population size N and the mutation rate, μ
168 (Figure 4C,D). In some cases it can also be affected by the fitness parameters (Figure S10).

Genetic instability in aneuploid cells. It has been suggested that aneuploidy increases genetic
170 instability: Sheltzer et al.⁵⁶ have demonstrated a fold increase of between 2.2 and 7.1 in mutation
rate. Therefore, we inferred model parameters under the assumption that the mutation rate increases
172 in aneuploid cells by a factor $\tau = 1, 33/32$ (due to an additional chromosome), 2, 5, 10, or 100 (due
to genetic instability). We found that the posterior distribution was similar for $\tau = 1, 33/32, 2$, and 5
174 (Figure S4). Furthermore, we computed the WAIC, a criterion for model selection (Methods). The
WAIC values were similar for all τ values (Table S1).

176 Assuming a strong increase of the mutation rate in aneuploid cells, i.e. $\tau = 100$, the inferred a
mutation rate was $\mu = 4.094 \cdot 10^{-7}$ [$6.252 \cdot 10^{-8} - 6.046 \cdot 10^{-7}$]), and the inferred aneuploidy rate
178 that was $\delta = 0.744 \cdot 10^{-3}$ [$0.506 \cdot 10^{-3} - 1.827 \cdot 10^{-3}$]. Compared to inference made assuming no
effect of aneuploidy on the mutation rate, these rates were about 7-8-fold and 2-3-fold lower for μ and
180 δ , respectively. Assuming $\tau = 10$, the inferred a mutation rate was only slightly lower compared to
 $\tau = 1$ ($\mu = 1.67 \cdot 10^{-6}$ [$2.836 \cdot 10^{-8} - 2.245 \cdot 10^{-6}$]).

182 Therefore, we do not find any evidence of an increase in mutation rate in aneuploid cells. This may
be because, unless the increase is strong ($\tau \geq 10$), it does not seem to affect our inference; or because
184 Chromosome III is one of the smallest chromosomes¹⁸. We also checked the differences in genotype
frequency dynamics for different τ values. We observe $\tau = 100$ could be distinguished if accurate
186 data was available for the waiting time until the frequency of $2n$ to decrease below 95% (Figure S5A)
or for waiting time for the frequency of $2n+1$ to either reach or go below 95% (Figure S5B). Similarly,
188 we did not find evidence for an increase in the rate of chromosome loss in aneuploid cells⁵⁶, probably
due to lack of statistical power.

190 Nevertheless, increasing the rate of chromosome loss (transitions from $2n+1^*$ to $2n^*$) without increasing
the rate of chromosome gain (transitions from $2n$ to $2n+1$) increases F_A (Figure S11B), but not to the
192 same extent as increasing the rate of chromosome gain. In contrast, increasing the mutation rate in
aneuploid cells can have a marked effect on the dynamics: when using the MAP parameter estimates,
194 F_A increases to 0.52 when the mutation rate in aneuploid cells increases 10-fold (Figure S11C).

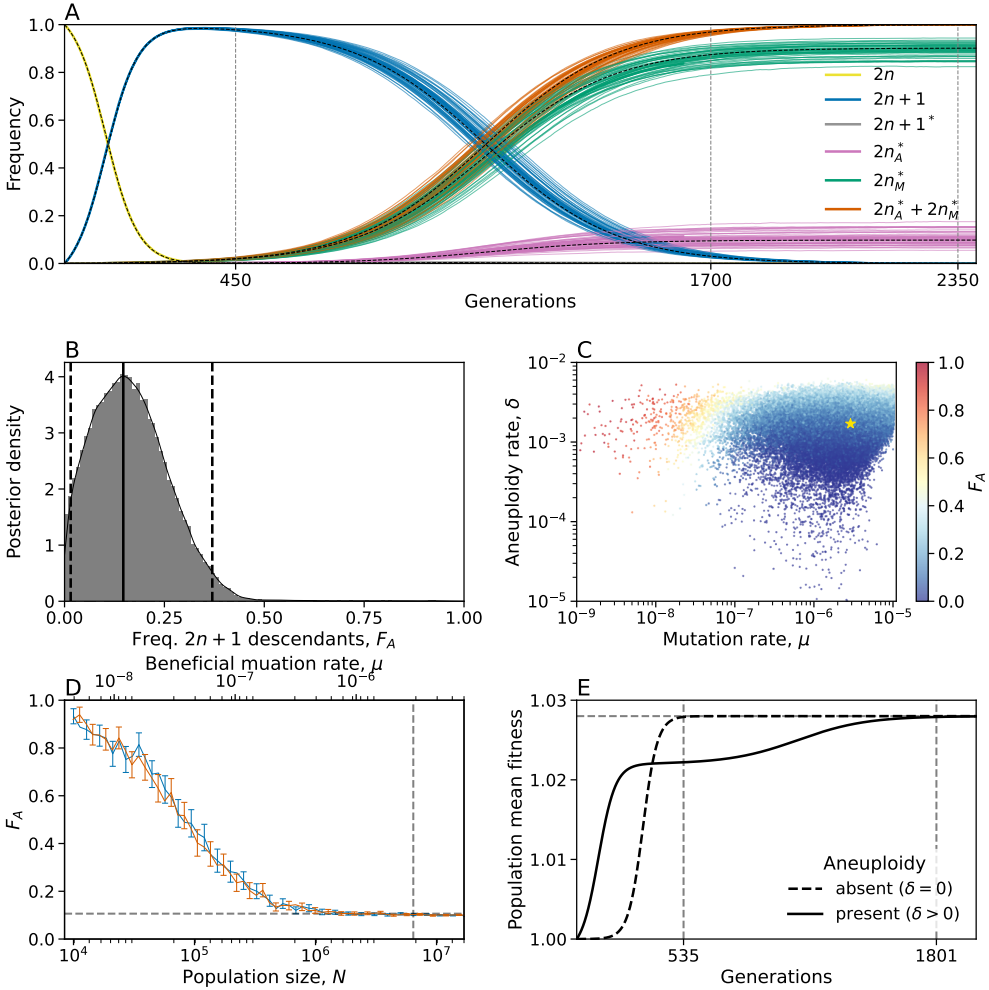


Figure 4: Predicted frequency of aneuploid-descended cells. **(A)** Posterior predicted genotype frequencies over time, including the source of $2n^*$: $2n_A^*$ arose from $2n+1$, whereas $2n_M^*$ arose directly from $2n$. Colored curves are 50 simulations using the MAP estimate parameters. Black dashed curves are the expected genotype frequencies without genetic drift (from a deterministic model). See Figure S9 for log-log scale, in which the sequence of events is easier to observe. **(B)** Posterior distribution of F_A , the expected frequency of $2n^*$ cells descended from $2n+1$ cells, computed as the average frequency at the end of 100 simulations for 100,000 samples from the parameter posterior distribution. Solid and dashed lines show the mode and 95% CI. **(C)** F_A values (color coded) from panel B, with their corresponding mutation rate μ on x-axis and aneuploidy rate δ on the y-axis. Yellow star shows the MAP estimate. See also Figure S10. **(D)** F_A as a function of the population size (N , bottom x-axis) and the beneficial mutation rate (μ , top x-axis) in posterior predictions with MAP parameters. Markers show F_A in 250 simulations per population size or mutation rate value. Error bars show mean F_A with 95% CI (bootstrap, $n = 10,000$). Blue and red bars for varying population size and mutation rate, respectively. Vertical dashed line for population size in the experiment, $6.425 \cdot 10^6$, and the MAP mutation rate, $2.965 \cdot 10^{-6}$. Horizontal line for $F_A^{MAP} = 0.106$. **(E)** Population mean fitness in a model without drift using MAP estimate parameters. Solid lines for mean fitness with aneuploidy ($\delta > 0$), where the population reaches adaptation (mean fitness at 99.99% of maximum value) at generation 1,802. Dashed lines for mean fitness without aneuploidy ($\delta = 0$), where the population adapts much earlier, at generation 535.

Discussion

196 In a study on the role of chromosome duplication in adaptive evolution, Yona et al.⁷⁰ found that a
197 Chromosome III trisomy was acquired by *S. cerevisiae* populations evolving under heat stress, only
198 to be later replaced by euploid mutant cells that carry "refined" solutions to the stress. Additionally,
199 such a replacement also occurred when they initiated evolutionary experiments with a population in
200 which all cells carry a Chromosome III trisomy. They hypothesized that aneuploidy is a "useful yet
201 short-lived intermediate that facilitates further adaptation", suggesting that the euploid mutant cells
202 evolved by heat-resistance mutations in aneuploid cells followed by reversion of trisomy due to a
203 chromosome loss event.

204 We developed an evolutionary genetic model of adaptive evolution by aneuploidy and mutation
(Figure 1), fitted it to the experimental results of Yona et al.⁷⁰, and used it to predict the genotype
205 frequency dynamics. The model predicted that only about 10-15% of the evolved euploid population
descended from aneuploid cells by acquiring a mutation and losing the extra chromosome—that is,
206 the majority of the euploid population are not descended from aneuploid cells, but rather are direct
207 descendants of the ancestral wild-type population (Figure 4).

210 This happens despite aneuploidy reaching a high frequency in the population (>95%). Conventional
211 wisdom might suggest that once the aneuploid genotype $2n+1$ reaches high frequency, it will have a
212 better chance at producing "refined" solutions via mutations, and its descendants will come to dominate
the population: the frequency of $2n_A^*$ (which arises from $2n+1^*$) will be higher than the frequency of
213 $2n_M^*$ (which arises directly from $2n$).

So how does $2n_M^*$ prevail? Initially, the supply rates of $2n+1$ and $2n_M^*$ are $N\delta \approx 11,000$ and $N\mu \approx 19$,
216 respectively (assuming MAP parameter estimates). Therefore, both genotypes are expected to appear
immediately at the beginning of the experiment (Figure S9). However, $2n+1$ appears at a much higher
218 frequency as $\delta \gg \mu$ by 2-3 orders of magnitude. After they first appear, $2n_M^*$ has higher fitness. But
as long as the frequency of $2n$ is high, the supply rate of $2n+1$ is higher than that of $2n_M^*$, again due to
220 $\delta \gg \mu$. However, supply rates of both genotypes decrease with the frequency of $2n$. Therefore, when
the latter decreases, mainly due to the increase in the frequency of $2n+1$, both supply rates diminish.
222 At this stage, the higher fitness of $2n_M^*$ comes into play and it starts to take over the population, which
is mainly composed of $2n+1$. For the aneuploid lineage to compete with the mutant lineage, it must
224 produce $2n_A^*$ via a mutation followed by chromosome loss. Although this is a stochastic process
(due to drift), our results show that the time until $2n_A^*$ reaches a frequency of 0.1% is roughly 450
226 generations, without much variation (intersection of purple lines and vertical dashed line in Figure S9).

However, by that time $2n_M^*$ is already at a roughly 10-fold higher frequency (1.86%), and since both mutants have the same fitness, their relative frequency remains roughly the same until the end of the experiment.

Predictions for small populations and low mutation rates. We examined the effect of the population size, N , and the beneficial mutation rate, μ , on the frequency of $2n+1$ descendants in the evolved population, F_A . We found that F_A is expected to decrease as the population size or mutation rate increase (Figure 4D), ranging from >90% when the population size is 10,000 or the mutation rate is $6 \cdot 10^{-9}$, to about 10% when the population size is above 1,000,000 (less than the experimental population size, which was 6,425,000) or the mutation rate is above $2 \cdot 10^{-6}$ (less than the inferred mutation rate, which is $2.965 \cdot 10^{-6}$). Thus, our model provides a testable prediction: if the experiment was repeated under a lower population size (via stronger daily dilutions or in a smaller volume) or a lower mutation rate (via a non-mutagenic stress or stress with a smaller target size such as drug resistance), then the fraction of the population descending from aneuploid cells would be much higher.

Aneuploidy delays rather than facilitates adaptation. An additional interesting result of our study is that aneuploidy increases, rather than decreases, the adaptation time (Figure 4E). This happens despite the fact that the mean fitness initially increases faster in the presence of aneuploidy (Figure 4E). This is because once $2n+1$ is common, selection for the mutant strain ($2n+1^*$ or $2n^*$) is weaker compared to when $2n^*$ competes directly with $2n$.

Rate and fitness effect of aneuploidy and mutation. We inferred the rates of aneuploidy and mutation and their effects on fitness. We estimate that the aneuploidy rate (i.e., number of chromosome gains per generation) is $1.7 \cdot 10^{-3}$, higher than a previous estimate of $6.7 \cdot 10^{-6}$ (ref⁷³). This may be due to genetic instability caused by heat stress⁵, but we note that there is a general scarcity of empirical data on aneuploidy rates. In addition, we find no evidence for increased mutation rates in aneuploid cells. Previous empirical studies have suggested that genetic instability (e.g., elevated mutation rates) in aneuploid cells is due to stress associated with the aneuploid state^{3,6,71,23}. However, in the experiment of Yona et al.⁷⁰, both the wild-type and the aneuploid were under heat stress, which may explain why we did not find evidence for an increased mutation rate specifically in aneuploid cells.

Conclusions. Here, we tested the hypothesis that aneuploidy cells are an evolutionary "stepping stone", or adaptive intermediate, between wild-type euploid cells and mutant euploid cells⁶⁹. Our results suggest that, although it seems the population goes from euploid to aneuploid and back, this is

258 not the case at the individual level. We estimate that only about 10-15% of the euploid cells descended
260 from aneuploid cells, whereas the rest are direct descendants of the wild-type euploid cells. Thus,
262 aneuploidy can delay, rather than accelerate, adaptation, and cells that become aneuploid may leave
264 less descendants than cells that remain euploid. This surprising result reinforces the importance of
mathematical models when interpreting evolutionary dynamics. Moreover, our study emphasizes the
unintuitive outcomes of clonal interference between mechanisms for generation of variation that differ
in their rate of formation and distribution of fitness effects, including mutation, copy number variation,
horizontal gene transfer, and epigenetic modifications.

266 Models and Methods

Evolutionary genetic model. We model the evolution of a population of cells using a Wright-Fisher model⁴⁰, assuming a constant effective population size N , non-overlapping generations, and including the effects of natural selection, genetic drift, aneuploidy, and mutation. We focus on beneficial genetic modifications, neglecting the effects of deleterious and neutral mutations or karyotypic changes. The model allows for a single aneuploid karyotype (e.g., Chromosome III duplication) and a single mutation to accumulate in the genotype. Thus, the model follows four genotypes (Figure 1): euploid wild-type, $2n$, the initial genotype; euploid mutant, $2n^*$, with the standard karyotype and a single beneficial mutation; aneuploid wild-type, $2n+1$, with an extra chromosome, i.e., following chromosome duplication; and aneuploid mutant, $2n+1^*$, with an extra chromosome and a beneficial mutation.

Transitions between the genotypes occur as follows (Figure 1): Beneficial mutations from $2n$ to $2n^*$ and from $2n+1$ to $2n+1^*$ occur with probability μ , the mutation rate. We neglect back-mutations (i.e., from $2n^*$ to $2n$ and from $2n+1^*$ to $2n+1$). Aneuploidy is formed by chromosome mis-segregation, so that cells transition from $2n$ to $2n+1$ and from $2n+1^*$ to $2n^*$ with probability δ , the aneuploidy rate. That is, we assume chromosomes are gained and lost at the same rate, and we neglect events that form a less-fit genotype (i.e., $2n+1$ to $2n$ and $2n^*$ to $2n+1^*$). A model that assumed increased rate of chromosome loss in aneuploid cells (as in Sheltzer et al.⁵⁶) did not perform well, probably due to lack of statistical power, and was abandoned.

In the experiment by Yona et al.⁷⁰, the population was grown every day from $1.6 \cdot 10^6$ cells until reaching stationary phase and then diluted 1:120. Thus, we set the population size to $N = 6.425 \cdot 10^6$, the harmonic mean of $\{2^k \cdot 1.6 \cdot 10^6\}_{k=0}^7$ ¹⁰. The initial population has N cells with genotype $2n$. The effect of natural selection on the frequency f_i of genotype $i = 2n, 2n + 1, 2n + 1^*$, or $2n^*$ is given

by

$$f_i^s = \frac{f_i w_i}{\bar{w}} , \quad (1)$$

where w_i is the fitness of genotype i and $\bar{w} = \sum_j f_j w_j$ is the population mean fitness. The effect of

mutation and aneuploidy on genotype frequencies is given by

$$\begin{aligned} f_{2n}^m &= (1 - \delta - \mu) f_{2n}^s , \\ f_{2n+1}^m &= \delta f_{2n}^s + (1 - \mu) f_{2n+1}^s , \\ f_{2n+1^*}^m &= \mu f_{2n+1}^s + (1 - \delta) f_{2n+1^*}^s , \\ f_{2n^*}^m &= \mu f_{2n}^s + \delta f_{2n+1^*}^s + f_{2n^*}^s . \end{aligned} \quad (2)$$

Finally, random genetic drift is modeled using a multinomial distribution⁴⁰,

$$\mathbf{f}' \sim \frac{1}{N} \cdot \text{Mult}(N, \mathbf{f}^m) , \quad (3)$$

where $\mathbf{f}^m = (f_{2n}^m, f_{2n+1}^m, f_{2n+1^*}^m, f_{2n^*}^m)$ are the frequencies of the genotypes after mutation and aneuploidy, \mathbf{f}' are the genotype frequencies in the next generation, and $\text{Mult}(N, \mathbf{f})$ is a multinomial distribution parameterized by the population size N and the genotype frequencies \mathbf{f} . Overall, the change in genotype frequencies from one generation to the next is given by the transformation $f_i \rightarrow f'_i$.

Empirical data for model inference. We use the results of evolutionary experiments reported by Yona et al.⁷⁰. In their heat-stress experiment, four populations of *S. cerevisiae* evolved under 39 °C. Aneuploidy fixed (frequency >95%) in all four population in the first 450 generations. Hereafter, fixation or elimination of a genotype by generation t means that more than 95% or less than 5% of the population carry the genotype at generation t , and possibly earlier. In the original analysis of Yona et al.⁷⁰, samples were routinely extracted from the evolving populations and tested for heat-shock tolerance. The first generation in which such indication was found was generation 200. Therefore, we determine that aneuploidy did not reach high frequency before generation 200. The experiment continued with two populations, in which aneuploidy was eliminated by generation 1,700 and 2,350 while still under the same conditions of elevated heat (39 °C).

Likelihood function. Because our model, just like the Wright-Fisher model, is non-linear and stochastic, computing the distribution of fixation time $T(g)$ of genotype g for use in the likelihood function is intractable (it is even hard to use a diffusion-equation approximation due to the model having multiple genotypes, rather than just two). We overcome this problem by approximating the likelihood using simulations. We simulate 1,000 experiments per parameter vector $\theta = (\mu, \delta, s, b, c)$, resulting

in a set of simulated observations $\tilde{\mathbf{X}} = \{\tilde{X}_i\}_{i=1}^{1000}$. We then compute the approximate likelihood,

$$\begin{aligned} \mathcal{L}(\theta) = P^4(200 \leq T(2n+1) \leq 450) \cdot & \left[1 - \right. \\ 316 \quad & P_{\tilde{\mathbf{X}}}^4(\{T(2n^*) < 1700\} \mid 200 \leq T(2n+1) \leq 450) - \\ & P_{\tilde{\mathbf{X}}}^4(\{1700 < T(2n^*) < 2350\} \mid 200 \leq T(2n+1) \leq 450) + \\ & \left. P_{\tilde{\mathbf{X}}}^4(\{T(2n^*) < 1700\} \wedge \{1700 < T(2n^*) < 2350\} \mid 200 \leq T(2n+1) \leq 450) \right], \end{aligned} \quad (4)$$

where $!\{\dots\}$ is the "logical not" operator, $P^4(\dots)$ is the 4th power of $P(\dots)$, and all probabilities

318 $P_{\tilde{\mathbf{X}}}(\dots)$ are approximated from the results of the simulations $\tilde{\mathbf{X}}$. For example, $P_{\tilde{\mathbf{X}}}(\{T(2n^*) < 1700\} \mid$

200 $\leq T(2n+1) \leq 450$) is approximated by taking simulations in which $2n+1$ fixed (reached >95%)

320 before generation 450 but not before generation 200, and computing the fraction of such simulations

in which $2n^*$ did not fix by generation 1,700, and hence aneuploidy did not extinct (reach <5%)

322 before generation 1,700. Figure S1 compares results with less and more simulated experiments,

demonstrating that 1,000 simulations are likely sufficient.

324 For a model without aneuploidy (that is, when the aneuploidy rate is fixed at zero, $\delta = 0$), we disregard

the increased expression in Chromosome III and the growth advantage measured in generation 450,

326 and focus on the growth advantage measured in later generations, presumably due to a beneficial

mutation. Therefore, the likelihood is approximated by

$$\begin{aligned} \mathcal{L}_!(\theta) = 1 - P_{\tilde{\mathbf{X}}}^4(\{T(2n^*) < 1700\}) - \\ 328 \quad P_{\tilde{\mathbf{X}}}^4(\{1700 < T(2n^*) < 2350\}) + \\ & P_{\tilde{\mathbf{X}}}^4(\{T(2n^*) < 1700\} \wedge \{1700 < T(2n^*) < 2350\}). \end{aligned} \quad (5)$$

Parameter inference. To infer model parameters, we use approximate Bayesian computation with

330 a sequential Monte-Carlo scheme, or ABC-SMC⁵⁹, implemented in the pyABC Python package²⁹

pyabc.readthedocs.io. This approach uses numerical stochastic simulations of the model to infer

332 a posterior distribution over the model parameters. It is a method of likelihood-free, simulation-

based inference⁹, that is, for estimating a posterior distribution when a likelihood function cannot be

334 directly computed. It is therefore suitable in our case, in which the likelihood function can only be

approximated from simulations, and cannot be directly computed.

336 The ABC-SMC algorithm employs sequential importance sampling over multiple iterations^{63,28,61}. In

iteration t of the algorithm, a set of parameter vectors, $\{\theta_{i,t}\}_{i=1}^{n_t}$, also called *particles*, are constructed

338 in the following way. A proposal particle, θ^* , is sampled from a proposal distribution, and is either

accepted or rejected, until n_t particles are accepted. The number of particles, n_t , is adapted at every

340 iteration t using the adaptive population strategy²⁹ pyabc.readthedocs.io. For $t = 0$, the proposal

particle is sampled from the prior distribution, $p(\theta)$. For $t > 0$, the proposal particle is sampled from
 342 the particles accepted in the previous iteration, $\{\theta_{i,t-1}\}_{i=1}^{n_{t-1}}$, each with a probability relative to its weight
 $W_{t-1}(\theta_{i,t-1})$ (see below). The proposal particle is then perturbed using a kernel perturbation kernel,
 344 $K_t(\theta^* | \theta)$ where θ is the sample from the previous iteration. Then, a set of synthetic observations
 $\tilde{\mathbf{X}}^*$ is simulated, and the proposal particle θ^* is accepted if its approximate likelihood (eq. (4)) is high
 346 enough, $\mathcal{L}(\theta^*) > 1 - \epsilon_t$ (or more commonly, if $1 - \mathcal{L}(\theta^*) < \epsilon_t$), where $\epsilon_t > 0$ is the *acceptance*
threshold, as higher values of ϵ_t allow more particles to be accepted. The acceptance threshold ϵ_t is
 348 chosen as the median of the $1 - \mathcal{L}(\theta)$ of the particles accepted in the previous iteration, $t - 1$, and
 $\epsilon_0 = 0.01$. For each accepted particle $\theta_{i,t}$ a weight $W_t(\theta_{i,t})$ is assigned: for $t = 0$, $W_0(\theta_{i,0}) = 1$,
 350 and for $t > 0$, $W_t(\theta_{i,t}) = p(\theta_{i,t}) / \sum_{i=1}^{n_{t-1}} W_{t-1}(\theta_{i,t-1}) K_t(\theta_{i,t}, \theta_{i,t-1})$, where $p(\theta)$ is the prior density of
 θ and $K_t(\theta', \theta)$ is the probability of a perturbation from θ to θ' . $K_t(\theta' | \theta)$ is a multivariate normal
 352 distribution, fitted at iteration t to the particles from the previous iteration, $\{\theta_{i,t-1}\}_{i=1}^{n_{t-1}}$, and their
 weights, $\{W(\theta_{i,t-1})\}_{i=1}^{n_{t-1}}$.
 354 Acceptance is determined according to the approximate likelihood (eq. (4)), which has a maximum
 value of $\mathcal{L}_{max} = 0.875$ (giving a minimal value of $\epsilon_{min} = 0.125$). We terminated the inference
 356 iterations when the change in ϵ value from one iteration to the next was small. With our standard prior
 and model, we reached $\epsilon = 0.13$ (or $\mathcal{L} = 0.87$) after six iterations, with $n_6 = 982$ accepted parameter
 358 vectors and effective sample size ESS=651 (Figure S2). Running the inference algorithm with different
 initialization seeds and less or more simulations for approximating the likelihood produced similar
 360 posterior distributions (Figure S1).

After producing a set of weighted particles from the the posterior distribution using the above ABC-
 362 SMC algorithm, we approximate the posterior using kernel density estimation (KDE) with Gaussian
 kernels. We truncate the estimated posterior to avoid positive posterior density for values with zero
 364 prior density. The MAP (maximum a posteriori) estimate is computed as the the maximum of the
 estimated joint posterior density. We then draw 5,000,000 samples from the posterior distribution
 366 to compute the HDI (highest density interval) and draw 50,000 samples to visualize the posterior
 distribution with histograms.

368 **Model comparison.** We examine several versions of our evolutionary models, e.g. without aneuploidy or with increased mutation rate in aneuploid cells, as well as several different prior distributions
 370 (see below). To compare these, we plot posterior predictions: for each model we execute 10,000
 simulations using the MAP parameter estimates and plot the distributions of time to fixation of $2n^*$,
 372 one of key properties of the model likelihood. These plots visualize the fit of each model to the

data. Also, for similar models we plot the marginal and joint posterior distributions of the parameters;

374 if these are similar, we consider the models interchangeable. We validate this by comparing HDI
(highest density interval) of posterior distributions.

376 Where posterior plots are very similar and the number of parameters is the same, we use WAIC, or
the widely applicable information criterion¹⁵, defined as

378
$$WAIC(\theta) = -2 \log \mathbb{E}[\mathcal{L}(\theta)] + 2\mathbb{V}[\log \mathcal{L}(\theta)] \quad (6)$$

where θ is a parameter vector, and $\mathbb{E}[\cdot]$ and $\mathbb{V}[\cdot]$ are the expectation and variance taken over the

380 posterior distribution, which in practice are approximated using 50,000 samples from the posterior
KDE. We validated that upon resampling WAIC values do not significantly change and that differences

382 in WAIC between models are preserved. WAIC values are scaled as a deviance measure: lower values
imply higher predictive accuracy.

384 **Prior distributions.** We used informative prior distributions for w_{2n+1} , w_{2n+1*} and w_{2n*} (we set
 $w_{2n} = 1$), which we estimated from growth curves data from mono-culture growth experiments

386 previously reported by Yona et al.⁷⁰, Figs. 3C, 4A, and S2. We used Curveball, a method
for predicting results of competition experiments from growth curve data⁴³ curveball.yoavram.com.

388 Briefly, Curveball takes growth curves of two strains growing separately in mono-culture and predicts
how they would grow in a mixed culture, that is, it predicts the results of a competition assay. From these
390 predictions, relative fitness values can be computed. Because Curveball uses a maximum-likelihood
approach to estimate model parameters, we were able to estimate a distribution of relative fitness
392 values to be used as a prior distribution by sampling 10,000 samples from a truncated multivariate
normal distribution defined by the maximum-likelihood covariance matrix (Figure S3).

394 We used growth curves of $2n$ and $2n+1$ in 39 °C to estimate an informative prior distribution for
 w_{2n+1} (Figure S3D, assuming $w_{2n} = 1$). In this prior distribution, we used the same prior for w_{2n+1*}

396 and w_{2n*} . To increase computational efficiency, we also assumed $w_{2n*} > w_{2n+1*} > w_{2n+1} > w_{2n}$;
running the inference without this assumption produced similar results. See *supporting material* for

398 an extended informative prior distribution that uses growth curves of $2n^*$ and $2n+1$ growing in 39 °C;
this prior distribution proved to be less useful.

400 As a control, we tested an uninformative uniform prior with $U(1, 6)$, for (i) all w_{2n+1} , w_{2n+1*} , w_{2n*} ,
or (ii) only for w_{2n+1*} , w_{2n*} , using the above informative prior for w_{2n+1} . In these cases the inference

402 algorithm failed to converge.

For the mutation rate, μ , and aneuploidy rate, δ , we used uninformative uniform priors, $\mu \sim$

404 $U(10^{-9}, 10^{-5})$ and $\delta \sim U(10^{-6}, 10^{-2})$. A wider mutation rate prior, $\mu \sim U(10^{-9}, 10^{-3})$, produced
similar results.

406 Acknowledgements

We thank Lilach Hadany, Judith Berman, David Gresham, Shay Covo, Martin Kupiec, Uri Obolski, Daniel
408 Weissman, and Tal Simon for discussions and comments. This work was supported in part by the Israel
Science Foundation (ISF, YR 552/19), the US-Israel Binational Science Foundation (BSF, YR 2021276),
410 Minerva Center for Live Emulation of Evolution in the Lab (YR, YP), Minerva Stiftung short-term research
grant (MP).

412 References

- [1] Avecilla, G., Chuong, J. N., Li, F., Sherlock, G., Gresham, D. and Ram, Y. 2022, ‘Neural networks enable efficient and accurate simulation-based inference of evolutionary parameters from adaptation dynamics’, *PLOS Biology* **20**(5), e3001633.
- 414 [2] Bakhoum, S. F. and Landau, D. A. 2017, ‘Chromosomal instability as a driver of tumor heterogeneity and evolution’, *Cold Spring Harb. Perspect. Med.* **7**(6), 1–14.
- 418 [3] Bouchonville, K., Forche, A., Tang, K. E. S., Semple, C. a. M. and Berman, J. 2009, ‘Aneuploid chromosomes are highly unstable during dna transformation of *Candida albicans*.’, *Eukaryot. Cell* **8**(10), 1554–66.
- 422 [4] Boveri, T. 2008, ‘Concerning the origin of malignant tumours’, *J. Cell Sci.* **121**(Supplement 1), 1–84.
- 424 [5] Chen, G., Bradford, W. D., Seidel, C. W. and Li, R. 2012, ‘Hsp90 stress potentiates rapid cellular adaptation through induction of aneuploidy.’, *Nature* **482**(7384), 246–50.
- 426 [6] Chen, G., Rubinstein, B. and Li, R. 2012, ‘Whole chromosome aneuploidy: Big mutations drive adaptation by phenotypic leap’, *BioEssays* **34**(10), 893–900.
- 428 [7] Cherry, J. M., Hong, E. L., Amundsen, C., Balakrishnan, R., Binkley, G., Chan, E. T., Christie, K. R., Costanzo, M. C., Dwight, S. S., Engel, S. R. et al. 2012, ‘Saccharomyces genome database: the genomics resource of budding yeast’, *Nucleic acids research* **40**(D1), D700–D705.
- 430 [8] Covo, S., Puccia, C. M., Argueso, J. L., Gordenin, D. A. and Resnick, M. A. 2014, ‘The sister

- chromatid cohesion pathway suppresses multiple chromosome gain and chromosome amplification.’, *Genetics* **196**(2), 373–384.
- [9] Cranmer, K., Brehmer, J. and Louppe, G. 2020, ‘The frontier of simulation-based inference’, *Proceedings of the National Academy of Sciences* p. 201912789.
- [10] Crow, J. F. and Kimura, M. 1970, *An introduction to population genetics theory*, Burgess Pub. Co., Minneapolis.
- [11] Dhar, R., Sägesser, R., Weikert, C., Yuan, J. and Wagner, A. 2011, ‘Adaptation of *Saccharomyces cerevisiae* to saline stress through laboratory evolution.’, *J. Evol. Biol.* **24**(5), 1135–53.
- [12] Dunham, M. J., Badrane, H., Ferea, T., Adams, J., Brown, P. O., Rosenzweig, F. and Botstein, D. 2002, ‘Characteristic genome rearrangements in experimental evolution of *Saccharomyces cerevisiae*’, *Proc. Natl. Acad. Sci.* **99**(25), 16144–16149.
- [13] Elde, Nels, C., Child, Stephanie, J., Eickbush, Michael, T., Kitzman, Jacob, O., Rogers, Kelsey, S., Shendure, J., Geballe, Adam, P. and Malik, Harmit, S. 2012, ‘Poxviruses deploy genomic accordions to adapt rapidly against host antiviral defenses’, *Cell* **150**(4), 831–841.
- [14] Flynn, J. M., Rossouw, A., Cote-Hammarlof, P., Fragata, I., Mavor, D., Hollins, C., Bank, C. and Bolon, D. N. 2020, ‘Comprehensive fitness maps of hsp90 show widespread environmental dependence’, *Elife* **9**, 1–25.
- [15] Gelman, A., Carlin, J. B., Stern, H. S., Dunson, D. B., Vehtari, A. and Rubin, D. B. 2013, *Bayesian Data Analysis, Third Edition*, Chapman & Hall/CRC Texts in Statistical Science, Taylor & Francis.
- [16] Gerstein, A. C. and Berman, J. 2020, ‘*Candida albicans* genetic background influences mean and heterogeneity of drug responses and genome stability during evolution in fluconazole’, *mSphere* **5**(3).
- [17] Gerstein, A. C., Ono, J., Lo, D. S., Campbell, M. L., Kuzmin, A. and Otto, S. P. 2015, ‘Too much of a good thing: the unique and repeated paths toward copper adaptation.’, *Genetics* **199**(2), 555–71.
- [18] Gilchrist, C. and Stelkens, R. 2019, ‘Aneuploidy in yeast: Segregation error or adaptation mechanism?’, *Yeast* **36**(9), 525–539.
- [19] Gresham, D., Desai, M. M., Tucker, C. M., Jenq, H. T., Pai, D. A., Ward, A., DeSevo, C. G.,

- 460 Botstein, D. and Dunham, M. J. 2008, ‘The repertoire and dynamics of evolutionary adaptations to controlled nutrient-limited environments in yeast’, *PLoS Genet.* **4**(12).
- 462 [20] Heidenreich, E. 2007, ‘Adaptive Mutation in *Saccharomyces cerevisiae*’, *Crit. Rev. Biochem. Mol. Biol.* **42**(4), 285–311.
- 464 [21] Hong, J. and Gresham, D. 2014, ‘Molecular specificity, convergence and constraint shape adaptive evolution in nutrient-poor environments’, *PLoS Genet.* **10**(1).
- 466 [22] Huang, C. J., Lu, M. Y., Chang, Y. W. and Li, W. H. 2018, ‘Experimental Evolution of Yeast for High-Temperature Tolerance’, *Mol. Biol. Evol.* **35**(8), 1823–1839.
- 468 [23] Ippolito, M. R., Martis, V., Martin, S., Tijhuis, A. E., Hong, C., Wardenaar, R., Dumont, M., Zerbib, J., Spierings, D. C., Fachinetti, D., Ben-David, U., Foijer, F. and Santaguida, S.
- 470 2021, ‘Gene copy-number changes and chromosomal instability induced by aneuploidy confer resistance to chemotherapy’, *Dev. Cell* **56**(17), 2440–2454.e6.
- 472 [24] Iwasa, Y., Michor, F. and Nowak, M. A. 2004, ‘Stochastic tunnels in evolutionary dynamics’, *Genetics* **166**(3), 1571–1579.
- 474 [25] Jarolim, S., Ayer, A., Pillay, B., Gee, A. C., Phrakaysone, A., Perrone, G. G., Breitenbach, M. and Dawes, I. W. 2013, ‘*Saccharomyces cerevisiae* genes involved in survival of heat shock’, *G3 Genes, Genomes, Genetics* **3**(12), 2321–2333.
- 476 [26] Kass, R. E. and Raftery, A. E. 1995, ‘Bayes factors’, *J. Am. Stat. Assoc.* **90**(430), 773.
- 478 [27] Kasuga, T., Bui, M., Bernhardt, E., Swiecki, T., Aram, K., Cano, L. M., Webber, J., Brasier, C., Press, C., Grünwald, N. J., Rizzo, D. M. and Garbelotto, M. 2016, ‘Host-induced aneuploidy and phenotypic diversification in the sudden oak death pathogen *Phytophthora ramorum*’, *BMC Genomics* **17**(1), 1–17.
- 482 [28] Klinger, E. and Hasenauer, J. 2017, A scheme for adaptive selection of population sizes in approximate bayesian computation - sequential monte carlo, in J. Feret and H. Koepll, eds, ‘Computational Methods in Systems Biology’, Vol. 10545, Springer International Publishing, pp. 128–144. Series Title: Lecture Notes in Computer Science.
- 484 [29] Klinger, E., Rickert, D. and Hasenauer, J. 2018, ‘pyabc: distributed, likelihood-free inference’, *Bioinformatics* (May), 1–3.
- 488 [30] Kohn, L. M. and Anderson, J. B. 2014, ‘The underlying structure of adaptation under strong selection in 12 experimental yeast populations’, *Eukaryot. Cell* **13**(9), 1200–1206.

- 490 [31] Komarova, N. L., Sengupta, A. and Nowak, M. A. 2003, ‘Mutation-selection networks of cancer
initiation: Tumor suppressor genes and chromosomal instability’, *Journal of Theoretical Biology*
492 **223**(4), 433–450.
- 494 [32] Kumaran, R., Yang, S.-Y. and Leu, J.-Y. 2013, ‘Characterization of chromosome stability in
diploid, polyploid and hybrid yeast cells’, *PLoS ONE* **8**(7), e68094.
- 496 [33] Lauer, S., Avecilla, G., Spealman, P., Sethia, G., Brandt, N., Levy, S. F. and Gresham, D. 2018,
‘Single-cell copy number variant detection reveals the dynamics and diversity of adaptation.’,
PLOS Biology **16**.
- 498 [34] Lukow, D. A., Sausville, E. L., Suri, P., Chunduri, N. K., Wieland, A., Leu, J., Smith, J. C., Girish,
V., Kumar, A. A., Kendall, J., Wang, Z., Storchova, Z. and Sheltzer, J. M. 2021, ‘Chromosomal
500 instability accelerates the evolution of resistance to anti-cancer therapies’, *Developmental Cell*
56(17), 2427–2439.e4.
- 502 [35] Lynch, M., Sung, W., Morris, K., Coffey, N., Landry, C. R., Dopman, E. B., Dickinson, W. J.,
Okamoto, K., Kulkarni, S., Hartl, D. L. and Thomas, W. K. 2008, ‘A genome-wide view of the
504 spectrum of spontaneous mutations in yeast’, *Proceedings of the National Academy of Sciences*
105(27), 9272–9277.
- 506 [36] Mannaert, A., Downing, T., Imamura, H. and Dujardin, J. C. 2012, ‘Adaptive mechanisms in
pathogens: Universal aneuploidy in *Leishmania*’, *Trends Parasitol.* **28**(9), 370–376.
- 508 [37] Möller, M., Habig, M., Freitag, M. and Stukenbrock, E. H. 2018, ‘Extraordinary genome
instability and widespread chromosome rearrangements during vegetative growth’, *Genetics*
510 **210**(2), 517–529.
- 512 [38] Naylor, R. M. and van Deursen, J. M. 2016, ‘Aneuploidy in cancer and aging’, *Annu. Rev. Genet.*
50(1), 45–66.
- 514 [39] Niwa, O., Tange, Y. and Kurabayashi, A. 2006, ‘Growth arrest and chromosome instability in
aneuploid yeast’, *Yeast* **23**(13), 937–950.
- 516 [40] Otto, S. P. and Day, T. 2007, *A biologist’s guide to mathematical modeling in ecology and
evolution*, Princeton University Press.
- 518 [41] Pavelka, N., Rancati, G., Zhu, J., Bradford, W. D., Saraf, A., Florens, L., Sanderson, B. W., Hat-
tem, G. L. and Li, R. 2010, ‘Aneuploidy confers quantitative proteome changes and phenotypic
variation in budding yeast.’, *Nature* **468**(7321), 321–5.

- 520 [42] Peter, J., De Chiara, M., Friedrich, A., Yue, J. X., Pflieger, D., Bergström, A., Sigwalt, A., Barre,
B., Freel, K., Llored, A., Cruaud, C., Labadie, K., Aury, J. M., Istance, B., Lebrigand, K., Barbry,
522 P., Engelen, S., Lemainque, A., Wincker, P., Liti, G. and Schacherer, J. 2018, ‘Genome evolution
across 1,011 *Saccharomyces cerevisiae* isolates’, *Nature* **556**(7701), 339–344.
- 524 [43] Ram, Y., Dellus-Gur, E., Bibi, M., Karkare, K., Obolski, U., Feldman, M. W., Cooper, T. F.,
Berman, J. and Hadany, L. 2019, ‘Predicting microbial growth in a mixed culture from growth
526 curve data’, *Proceedings of the National Academy of Sciences* **116**(29), 14698–14707.
- 528 [44] Rancati, G., Pavelka, N., Fleharty, B., Noll, A., Trimble, R., Walton, K., Perera, A., Staehling-
Hampton, K., Seidel, C. W. and Li, R. 2008, ‘Aneuploidy underlies rapid adaptive evolution of
yeast cells deprived of a conserved cytokinesis motor’, *Cell* **135**(5), 879–893.
- 530 [45] Robbins, N., Caplan, T. and Cowen, L. E. 2017, ‘Molecular evolution of antifungal drug resis-
tance’, *Annu. Rev. Microbiol.* **71**(1), 753–775.
- 532 [46] Robinson, D., Vanacloig-Pedros, E., Cai, R., Place, M., Hose, J. and Gasch, A. P. 2023, ‘Gene-
by-environment interactions influence the fitness cost of gene copy-number variation in yeast’,
534 *bioRxiv*.
- 536 [47] Rodrigues, M. L. and Albuquerque, P. C. 2018, ‘Searching for a change: The need for increased
support for public health and research on fungal diseases’, *PLoS Negl. Trop. Dis.* **12**(6), 1–5.
- 538 [48] Rutledge, S. D., Douglas, T. A., Nicholson, J. M., Vila-Casadesús, M., Kantzler, C. L., Wangsa,
D., Barroso-Vilares, M., Kale, S. D., Logarinho, E. and Cimini, D. 2016, ‘Selective advantage of
trisomic human cells cultured in non-standard conditions’, *Scientific Reports* **6**(June 2015), 1–12.
- 540 [49] Santaguida, S. and Amon, A. 2015, ‘Short- and long-term effects of chromosome mis-segregation
and aneuploidy’, *Nat. Rev. Mol. Cell Biol.* **16**(8), 473–485.
- 542 [50] Santaguida, S., Vasile, E., White, E. and Amon, A. 2015, ‘Aneuploidy-induced cellular stresses
limit autophagic degradation’, *Genes Dev.* **29**(19), 2010–2021.
- 544 [51] Schwartzman, J. M., Sotillo, R. and Benezra, R. 2010, ‘Mitotic chromosomal instability and
cancer: Mouse modelling of the human disease’, *Nat. Rev. Cancer* **10**(2), 102–115.
- 546 [52] Selmecki, A. M., Dulmage, K., Cowen, L. E., Anderson, J. B. and Berman, J. 2009, ‘Acquisition
of aneuploidy provides increased fitness during the evolution of antifungal drug resistance’, *PLoS
548 Genet.* **5**(10), e1000705.

- 550 [53] Selmecki, A. M., Forche, A. and Berman, J. 2010, ‘Genomic plasticity of the human fungal pathogen *Candida albicans*’, *Eukaryot. Cell* **9**(7), 991–1008.
- 552 [54] Selmecki, A. M., Gerami-Nejad, M., Paulson, C., Forche, A. and Berman, J. 2008, ‘An isochromosome confers drug resistance in vivo by amplification of two genes, erg11 and tac1’, *Mol. Microbiol.* **68**(3), 624–641.
- 554 [55] Sheltzer, J. M. and Amon, A. 2011, ‘The aneuploidy paradox: Costs and benefits of an incorrect karyotype’, *Trends Genet.* **27**(11), 446–453.
- 556 [56] Sheltzer, J. M., Blank, H. M., Pfau, S. J., Tange, Y., George, B. M., Humpton, T. J., Brito, I. L., Hiraoka, Y., Niwa, O. and Amon, A. 2011, ‘Aneuploidy drives genomic instability in yeast’, *Science* **333**(6045), 1026–1030.
- 560 [57] Sheltzer, J. M., Ko, J. H., Replogle, J. M., Habibe Burgos, N. C., Chung, E. S., Meehl, C. M., Sayles, N. M., Passerini, V., Storchova, Z. and Amon, A. 2017, ‘Single-chromosome gains commonly function as tumor suppressors’, *Cancer Cell* **31**(2), 240–255.
- 562 [58] Sionov, E., Lee, H., Chang, Y. C. and Kwon-Chung, K. J. 2010, ‘*Cryptococcus neoformans* overcomes stress of azole drugs by formation of disomy in specific multiple chromosomes’, *PLoS Pathog.* **6**(4), e1000848.
- 566 [59] Sisson, S. A., Fan, Y. and Tanaka, M. M. 2007, ‘Sequential monte carlo without likelihoods’, *Proceedings of the National Academy of Sciences* **104**(6), 1760–1765.
- 568 [60] Sonti, R. V. and Roth, J. R. 1989, ‘Role of gene duplications in the adaptation of *Salmonella typhimurium* to growth on limiting carbon sources.’, *Genetics* **123**(1), 19–28.
- 570 [61] Syga, S., David-Rus, D., Schälte, Y., Hatzikirou, H. and Deutsch, A. 2021, ‘Inferring the effect of interventions on covid-19 transmission networks’, *Scientific Reports* **11**(1), 1–11.
- 572 [62] Todd, R. T., Forche, A. and Selmecki, A. M. 2017, ‘Ploidy variation in fungi: Polyploidy, aneuploidy, and genome evolution’, *Microbiol. Spectr.* **5**(4), 1–20.
- 574 [63] Toni, T., Welch, D., Strelkowa, N., Ipsen, A. and Stumpf, M. P. 2009, ‘Approximate bayesian computation scheme for parameter inference and model selection in dynamical systems’, *J. R. Soc. Interface* **6**(31), 187–202.
- 576 [64] Torres, E. M., Dephoure, N., Panneerselvam, A., Tucker, C. M., Whittaker, C. A., Gygi, S. P., Dunham, M. J. and Amon, A. 2010, ‘Identification of aneuploidy-tolerating mutations’, *Cell* **143**(1), 71–83.

- [65] Torres, E. M., Sokolsky, T., Tucker, C. M., Chan, L. Y., Boselli, M., Dunham, M. J. and Amon, A. 2007, ‘Effects of aneuploidy on cellular physiology and cell division in haploid yeast’, *Science* (80-.). **317**(5840), 916–924.
- [66] Tsai, H. J., Nelliat, A. R., Choudhury, M. I., Kucharavy, A., Bradford, W. D., Cook, M. E., Kim, J., Mair, D. B., Sun, S. X., Schatz, M. C. and Li, R. 2019, ‘Hypo-osmotic-like stress underlies general cellular defects of aneuploidy’, *Nature* .
- [67] Williams, B. R., Prabhu, V. R., Hunter, K. E., Glazier, C. M., Whittaker, C. a., Housman, D. E. and Amon, A. 2008, ‘Aneuploidy affects proliferation and spontaneous immortalization in mammalian cells’, *Science* **322**(5902), 703–709.
- [68] Yang, F., Todd, R. T., Selmecki, A., Jiang, Y. Y., Cao, Y. B. and Berman, J. 2021, ‘The fitness costs and benefits of trisomy of each *Candida albicans* chromosome’, *Genetics* **218**(2), 1–7.
- [69] Yona, A. H., Frumkin, I. and Pilpel, Y. 2015, ‘A relay race on the evolutionary adaptation spectrum’, *Cell* **163**(3), 549–559.
- [70] Yona, A. H., Manor, Y. S., Herbst, R. H., Romano, G. H., Mitchell, A., Kupiec, M., Pilpel, Y. and Dahan, O. 2012, ‘Chromosomal duplication is a transient evolutionary solution to stress.’, *Proceedings of the National Academy of Sciences* **109**(51), 21010–5.
- [71] Zhu, J., Pavelka, N., Bradford, W. D., Rancati, G. and Li, R. 2012, ‘Karyotypic determinants of chromosome instability in aneuploid budding yeast’, *PLoS Genetics* **8**(5).
- [72] Zhu, J., Tsai, H.-J., Gordon, M. R. and Li, R. 2018, ‘Cellular stress associated with aneuploidy’, *Dev. Cell* **44**(4), 420–431.
- [73] Zhu, Y. O., Sherlock, G. and Petrov, D. A. 2016, ‘Whole genome analysis of 132 clinical *Saccharomyces cerevisiae* strains reveals extensive ploidy variation’, *G3 Genes, Genomes, Genetics* **6**(8), 2421–2434.
- [74] Zhu, Y. O., Siegal, M. L., Hall, D. W. and Petrov, D. A. 2014, ‘Precise estimates of mutation rate and spectrum in yeast’, *Proceedings of the National Academy of Sciences* **111**(22), E2310–E2318.

604 Supplementary Material

Supplementary Analysis

606 **Sensitivity analysis.** Changing a single parameter while keeping the rest fixed at the MAP estimate produces a worse fit to the data (Figure S6). Furthermore, we fitted models with a mutation rate
608 fixed at $\mu = 10^{-5}$, 10^{-6} and 10^{-7} . We inferred similar parameters estimates for the model with
 $\mu = 10^{-6}$ compared to the model with a free μ parameter, in which the inferred mutation rate is
610 $\mu \approx 3 \cdot 10^{-6}$. Inference assuming $\mu = 10^{-5}$ or $\mu = 10^{-7}$ produced similar estimates except that the
estimated aneuploidy rate, δ , was higher, and assuming $\mu = 10^{-7}$, the estimated fitness of $2n+1$ was
612 lower (Figure S7).

614 **Extended informative prior distribution.** In an extended informative prior distribution, we used
additional growth curves of $2n^*$ (*refined* strain from Yona et al.⁷⁰) and $2n+1$ in 39 °C to estimate
616 w_{2n^*}/w_{2n+1} (Figure S3H). The same distribution was used for w_{2n^*}/w_{2n+1*} . Thus, our main informative prior uses a single prior distribution for fitness values of $2n+1$, $2n+1^*$, and $2n^*$, whereas the extended informative prior uses one distribution for $2n+1$, and another distribution for both $2n+1^*$
618 and $2n^*$.

We estimated the parameters under this extended informative prior. Inference took much longer
620 to run but the posterior distribution seemed to converge, as it did not change much in the final iterations. The posterior predictive plot shows that inference with this extended prior produces a
622 posterior distribution that fails to explain the empirical observations (pink in Figure 3). However, the inferred posterior distribution is considerably narrower (compare Figures 2 and S8) and therefore
624 parameter estimates are less variable. The estimated mutation rate was much lower compared to the main informative prior, with $\mu = 2.474 \cdot 10^{-9}$ [$2.423 \cdot 10^{-9} - 2.612 \cdot 10^{-9}$]. Other parameter
626 estimates are: $\delta = 2.705 \cdot 10^{-3}$ [$2.094 \cdot 10^{-3} - 3.094 \cdot 10^{-3}$], $w_{2n+1} = 1.022$ [$1.021 - 1.024$],
 $w_{2n+1*} = 1.052$ [$1.05 - 1.054$], $w_{2n^*} = 1.053$ [$1.051 - 1.055$], the latter two being much higher
628 compare to the main informative prior. Notably, the mode of the posterior ratio $w_{2n^*}/w_{2n+1} = 1.0009$ is much lower than the mode of the prior ratio of 1.033 (Figure S3H) and closer to the ratio of 1 that
630 we assume in the main informative prior. Together with the posterior predictive results, we conclude that the main informative prior is preferable over the extended informative prior.

632 **Model with transitions to less-fit genotypes** We also estimated the parameters of a version of the model that includes transitions (mutation, chromosome loss and gain) to less-fit genotypes (e.g., $2n^*$

634 to $2n+1^*$),

$$\begin{aligned}
 f_{2n}^m &= (1 - \delta - \mu)f_{2n}^s + \delta f_{2n+1}^s + \mu f_{2n^*}^s , \\
 f_{2n+1}^m &= \delta f_{2n}^s + (1 - \delta - \mu)f_{2n+1}^s + \mu f_{2n+1^*}^s , \\
 f_{2n+1^*}^m &= \mu f_{2n+1}^s + (1 - \delta - \mu)f_{2n+1^*}^s + \delta f_{2n^*}^s , \\
 f_{2n^*}^m &= \mu f_{2n}^s + \delta f_{2n+1^*}^s + (1 - \delta - \mu)f_{2n^*}^s .
 \end{aligned} \tag{7}$$

636 The inferred values are slightly different. The estimated mutation rate, $\mu = 1.036 \cdot 10^{-7}$ [$8.01 \cdot 10^{-8} - 1.339 \cdot 10^{-7}$], corresponds to a mutation target size of $\sim 300 - 500$, assuming the mutation
 638 rate per base pair is roughly $2 \cdot 10^{-10}$ (ref.⁷⁴) or $3.3 \cdot 10^{-10}$ (ref.³⁵). The estimated aneuploidy
 640 rate, $\delta = 2.358 \cdot 10^{-4}$ [$1.766 \cdot 10^{-4} - 2.837 \cdot 10^{-4}$] is 5-35-fold higher than in previous studies:
 642 for Chromosome III in diploid *S. cerevisiae*, Zhu et al.⁷⁴ estimated $6.7 \cdot 10^{-6}$ chromosome gain
 events per generation, and Kumaran et al.³² estimate $3.0 - 4.3 \cdot 10^{-5}$ chromosome loss events per
 644 generation (95% confidence interval). The estimated fitness values are $w_{2n+1} = 1.024$ [$1.023 - 1.025$],
 $w_{2n+1^*} = 1.025$ [$1.024 - 1.026$], $w_{2n^*} = 1.032$ [$1.031 - 1.033$], all relative to the fitness of $2n$, which

is set to $w_{2n} = 1$.

We simulated genotype frequency dynamics using parameter samples from the posterior distribution,
 646 and computed the posterior distribution of F_A . The mean F_A in this case is just 0.0189 [0.0004 -
 0.1214 95% CI], lower than without the transitions to less-fit genotypes. Here, F_A is the sum of
 648 frequencies of both $2n_A^*$ and $2n + 1_A^*$, which reaches a frequency of 0.0007. Out of 100,000 posterior
 samples, none had F_A above 0.05 (i.e., 5% of the population).

650 **Supplementary Figures & Tables**

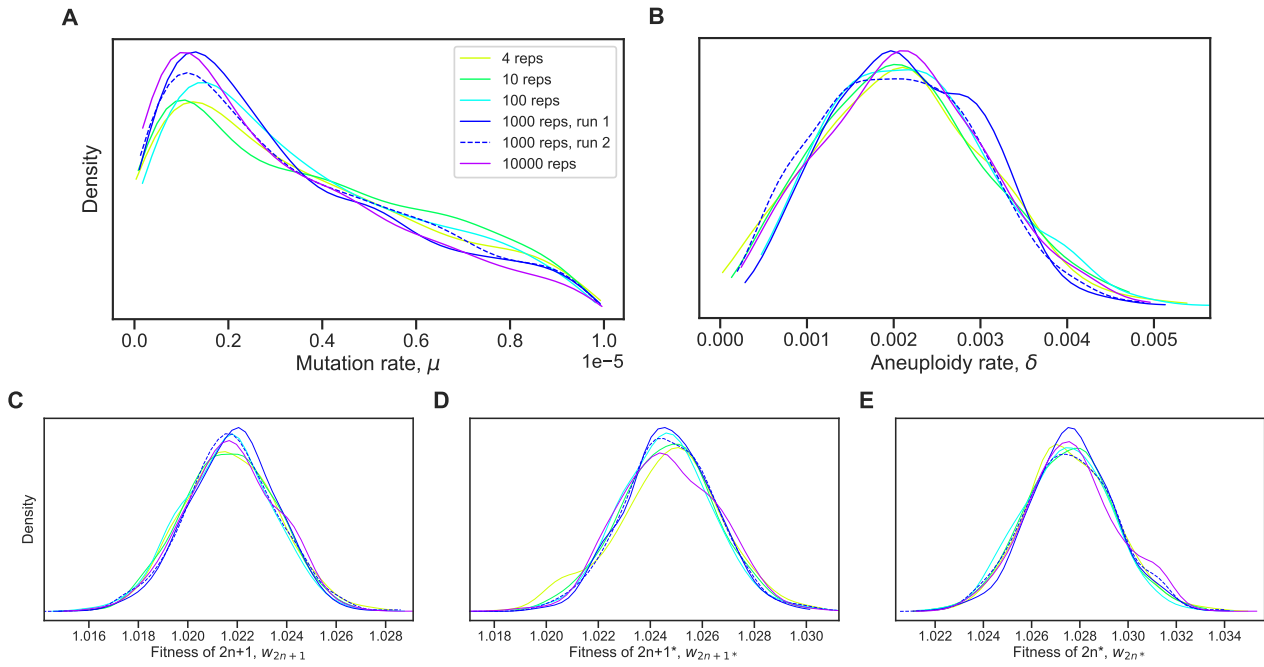


Figure S1: Posterior distribution validation. The posterior distribution of model parameters is roughly the same regardless of the number of simulations (4-10,000 replicates) used to approximate the likelihood (eq. (4)).

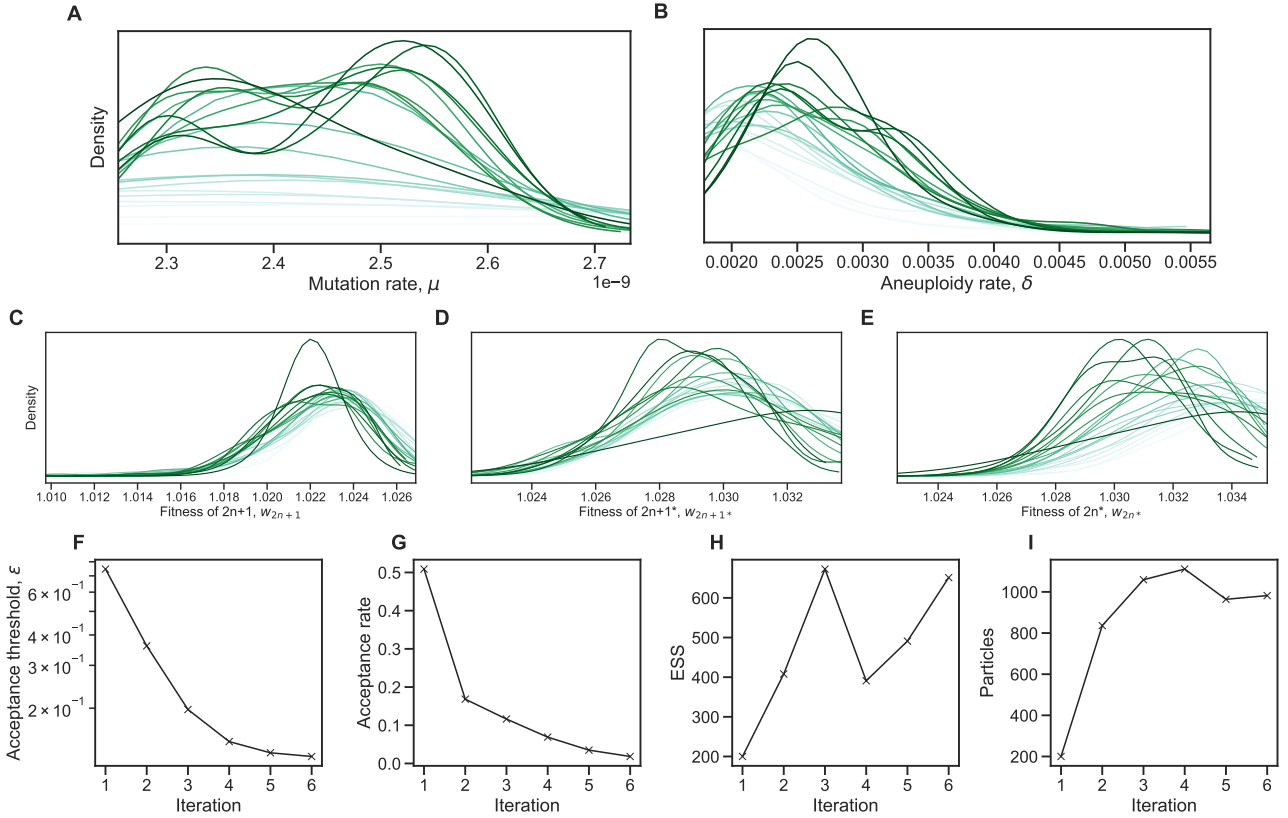


Figure S2: Inference convergence. The ABC-SMC algorithm was used to infer the model parameters. **(A-E)** The approximate posterior distributions of model parameters at each iteration of the ABC-SMC algorithm demonstrates convergence, as the posterior did not significantly change after the first iteration, $t = 1$. **(F-I)** ABC-SMC measures of convergence. After iteration number 6, the acceptance threshold was $\epsilon = 0.13$ (i.e., $\mathcal{L} = 0.87$, eq. (4)), the acceptance rate was 0.018, the number of particles was 982, and the effective sample size ESS=651.

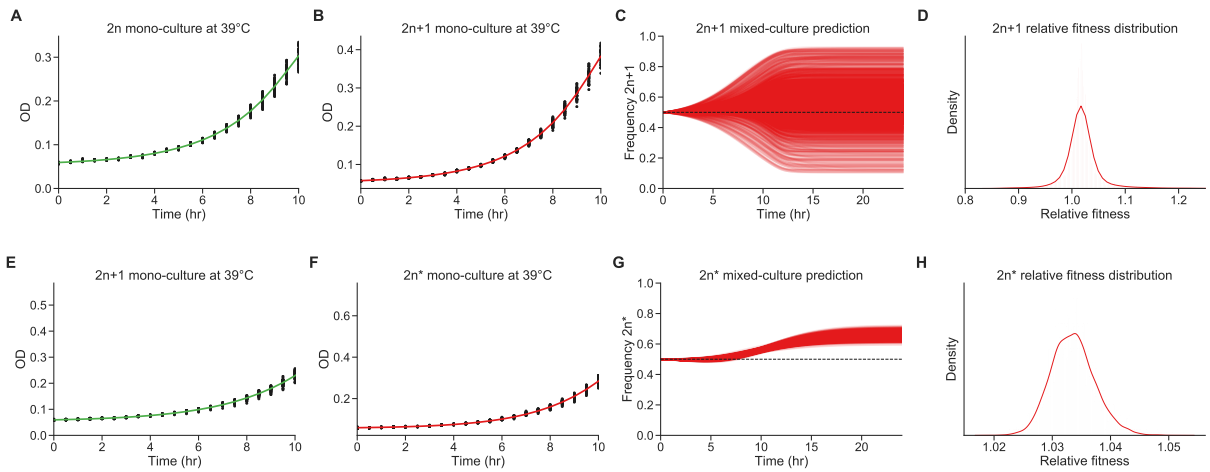


Figure S3: Fitness estimation from growth curves. **(A-D)** Fitness estimation from growth curves of $2n$ and $2n+1$ at 39°C . $w_{2n+1}/w_{2n}=1.024$ (95% CI: 0.959 - 1.115). **Curveball (E-H)** Fitness estimation from growth curves of $2n+1$ and $2n^*$ at 39°C . $w_{2n^*}/w_{2n+1}=1.033$ (95% CI: 1.027 - 1.041). Growth curves previously described in Yona et al.⁷⁰, Figs. 3C, 4A, and S2. Fitness estimated from growth curves using Curveball, a method for predicting results of competition experiments from growth curve data⁴³ curveball.yoavram.com. See *Models and Methods, Prior distributions* for more details. **(A,B;E,F)** Mono-culture growth curve data (markers) and best-fit growth models (lines). **(C,G)** The mixed-culture prediction for the strains from A,B and E,F respectively, 6,375 generated curves. **(D,H)** The relative fitness distribution for $2n+1$ relative to $2n$ (panel D) and $2n^*$ relative to $2n+1$ (panel H). Figures generated by Curveball.

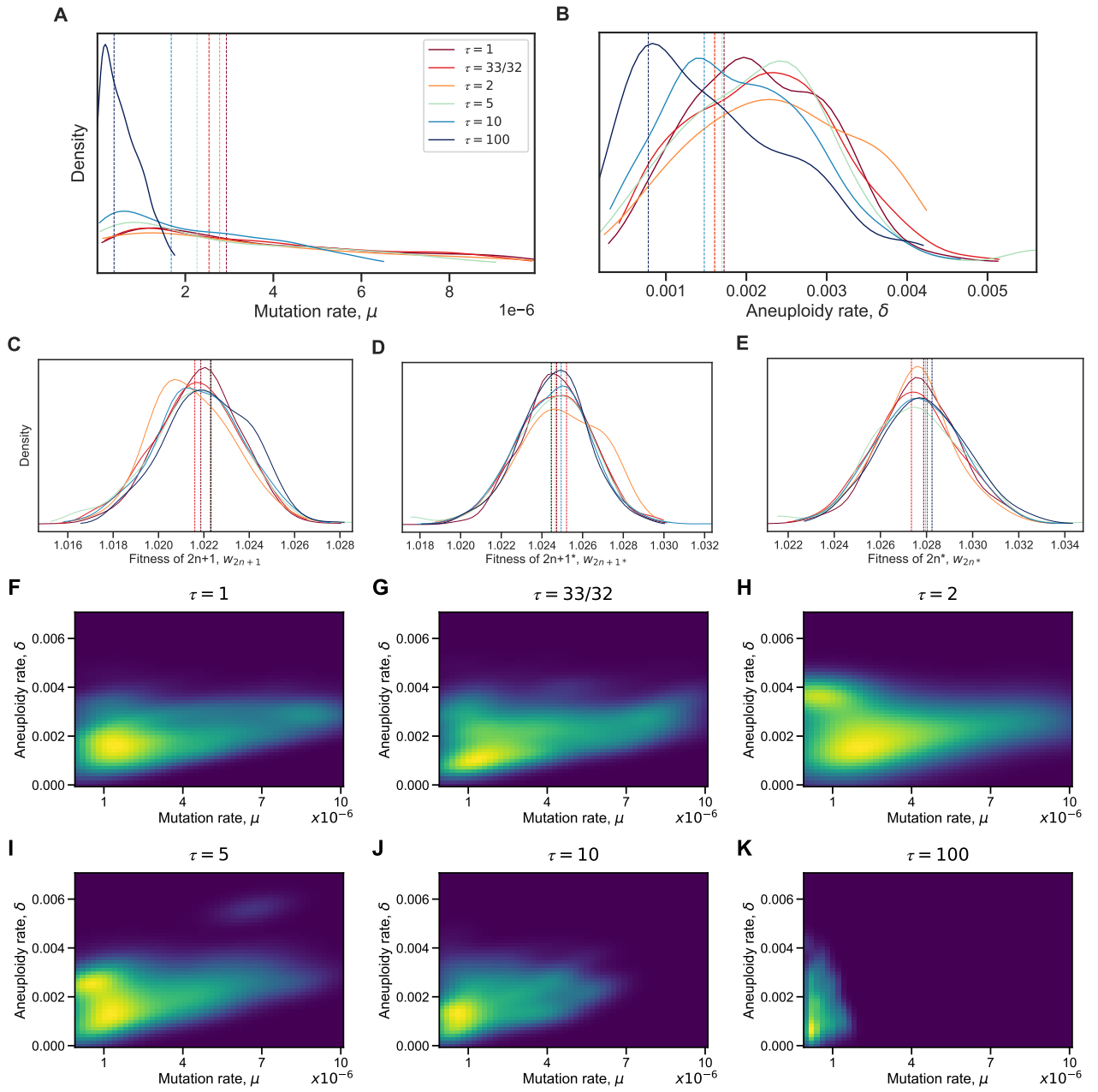


Figure S4: Model with elevated mutation rate in aneuploid cells. (A-E) The inferred posterior distributions for models with different values of τ , the fold-increase in mutation rate in aneuploid cells ($2n+1$ and $2n+1^*$). Vertical dashed lines represent the MAP (maximum a posteriori) of each distribution. When the increase in mutation rate is high, $\tau = 10$ and $\tau = 100$, the inferred mutation (A) and aneuploidy (B) rates tend to be lower. (F-K) The inferred joint posterior distribution of mutation rate (μ) and aneuploidy rate (δ) with different τ values (dark purple and bright yellow for low and high density, respectively).

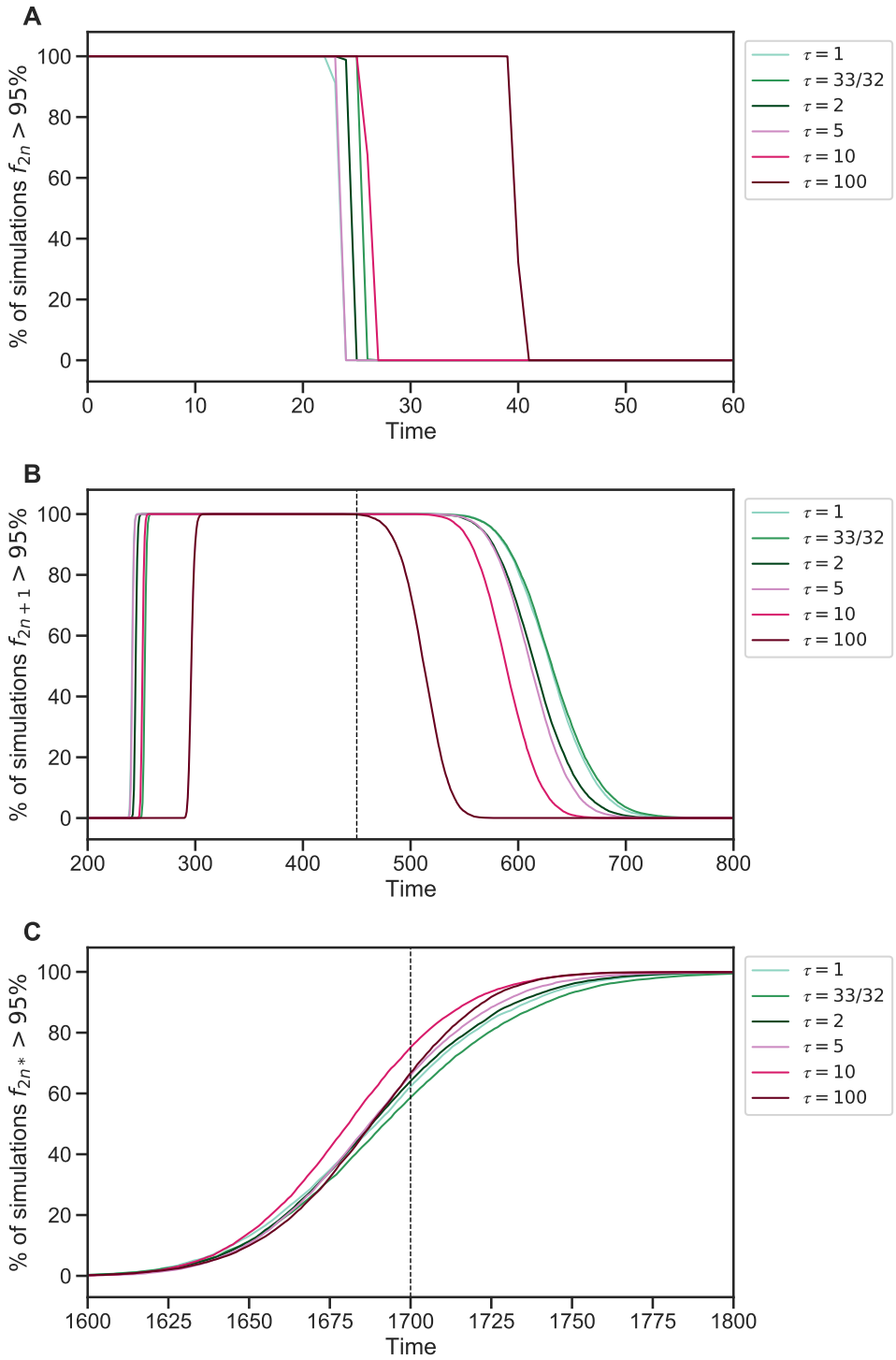


Figure S5: Genotype fixations for models with increased genetic instability. We estimated the parameters for different models, each assuming a different value of τ , the fold-increase in mutation rate in aneuploid cells. We then generated 10,000 simulations using the MAP estimate of each model and evaluated the fraction of simulations in which the frequency of genotype $2n$ (**A**), $2n+1$ (**B**), and $2n^*$ (**C**) is above 95% (y-axis) at each generation (x-axis). Note that $2n+1^*$ did not fix. We can see that $\tau = 100$ can be distinguished if the waiting time for $f_{2n} < 95\%$ is known (panel A) or if the waiting time for $f_{2n+1} > 95\%$ or $f_{2n+1} < 95\%$ is known (panel B). It is harder to distinguish between $1 \leq \tau \leq 10$.

Table S1: WAIC values for different τ values. Differences of less than 6 are considered of weak significance²⁶.

Model	WAIC
$\tau = 1$	-9
$\tau = 33/32$	-9
$\tau = 2$	-8
$\tau = 5$	-12
$\tau = 10$	-9
$\tau = 100$	-12

WAIC defined in eq. (6).

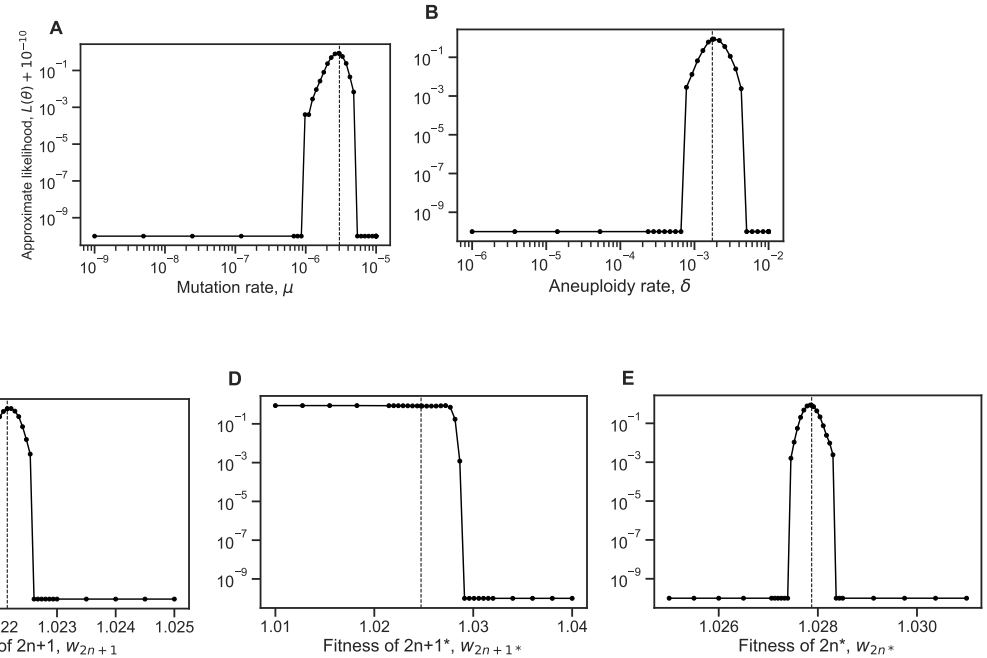


Figure S6: Likelihood profiles. Sensitivity of the model approximate likelihood, $\mathcal{L}(\theta)$, to changing a single parameter while the other parameters remain fixed at their MAP estimates. Dashed vertical line represents the MAP value. The prior distributions for the mutation rate and aneuploidy rate are $\mu \sim U(10^{-9}, 10^{-5})$ and $\delta \sim U(10^{-6}, 10^{-2})$, respectively.

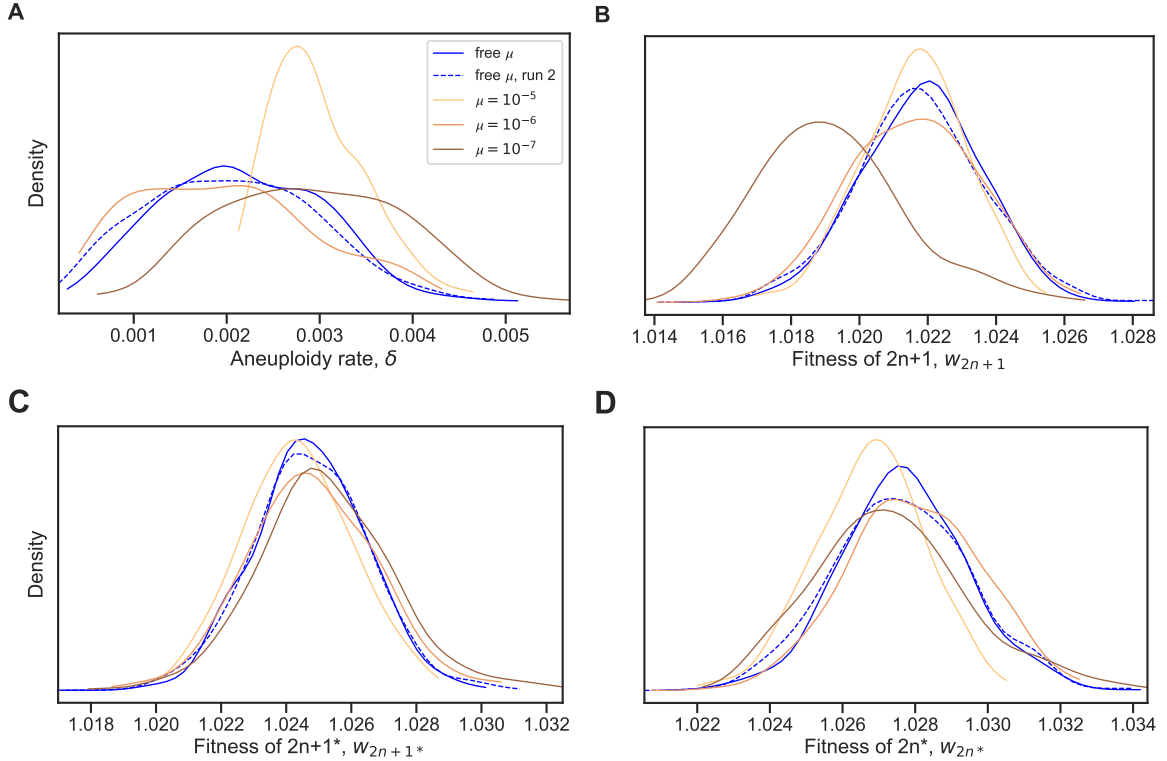


Figure S7: Model with fixed mutation rate. (A-D) The inferred posterior distributions for models with free and fixed mutation rate, μ . The MAP (maximum a posteriori) and 50% HDI (highest density interval) for each model are: **free μ , run 1:** $\delta = 1.720 \cdot 10^{-3}$ [$1.470 \cdot 10^{-3} - 2.786 \cdot 10^{-3}$], $w_{2n+1} = 1.022$ [1.021 – 1.023], $w_{2n+1^*} = 1.025$ [1.024 – 1.026], $w_{2n^*} = 1.028$ [1.026 – 1.029]; **free μ , run 2:** $\delta = 2.129 \cdot 10^{-3}$ [$1.334 \cdot 10^{-3} - 2.695 \cdot 10^{-3}$], $w_{2n+1} = 1.022$ [1.02 – 1.023], $w_{2n+1^*} = 1.025$ [1.023 – 1.026], $w_{2n^*} = 1.028$ [1.026 – 1.029]; **$\mu = 10^{-5}$:** $\delta = 2.903 \cdot 10^{-3}$ [$2.399 \cdot 10^{-3} - 3.156 \cdot 10^{-3}$], $w_{2n+1} = 1.022$ [1.021 – 1.023], $w_{2n+1^*} = 1.024$ [1.023 – 1.025], $w_{2n^*} = 1.027$ [1.026 – 1.028]; **$\mu = 10^{-6}$:** $\delta = 1.917 \cdot 10^{-3}$ [$9.624 \cdot 10^{-4} - 2.447 \cdot 10^{-3}$], $w_{2n+1} = 1.022$ [1.02 – 1.023], $w_{2n+1^*} = 1.025$ [1.023 – 1.026], $w_{2n^*} = 1.028$ [1.027 – 1.029]; **$\mu = 10^{-7}$:** $\delta = 2.901 \cdot 10^{-3}$ [$2.139 \cdot 10^{-3} - 3.671 \cdot 10^{-3}$], $w_{2n+1} = 1.019$ [1.017 – 1.02], $w_{2n+1^*} = 1.025$ [1.024 – 1.026], $w_{2n^*} = 1.027$ [1.026 – 1.029].

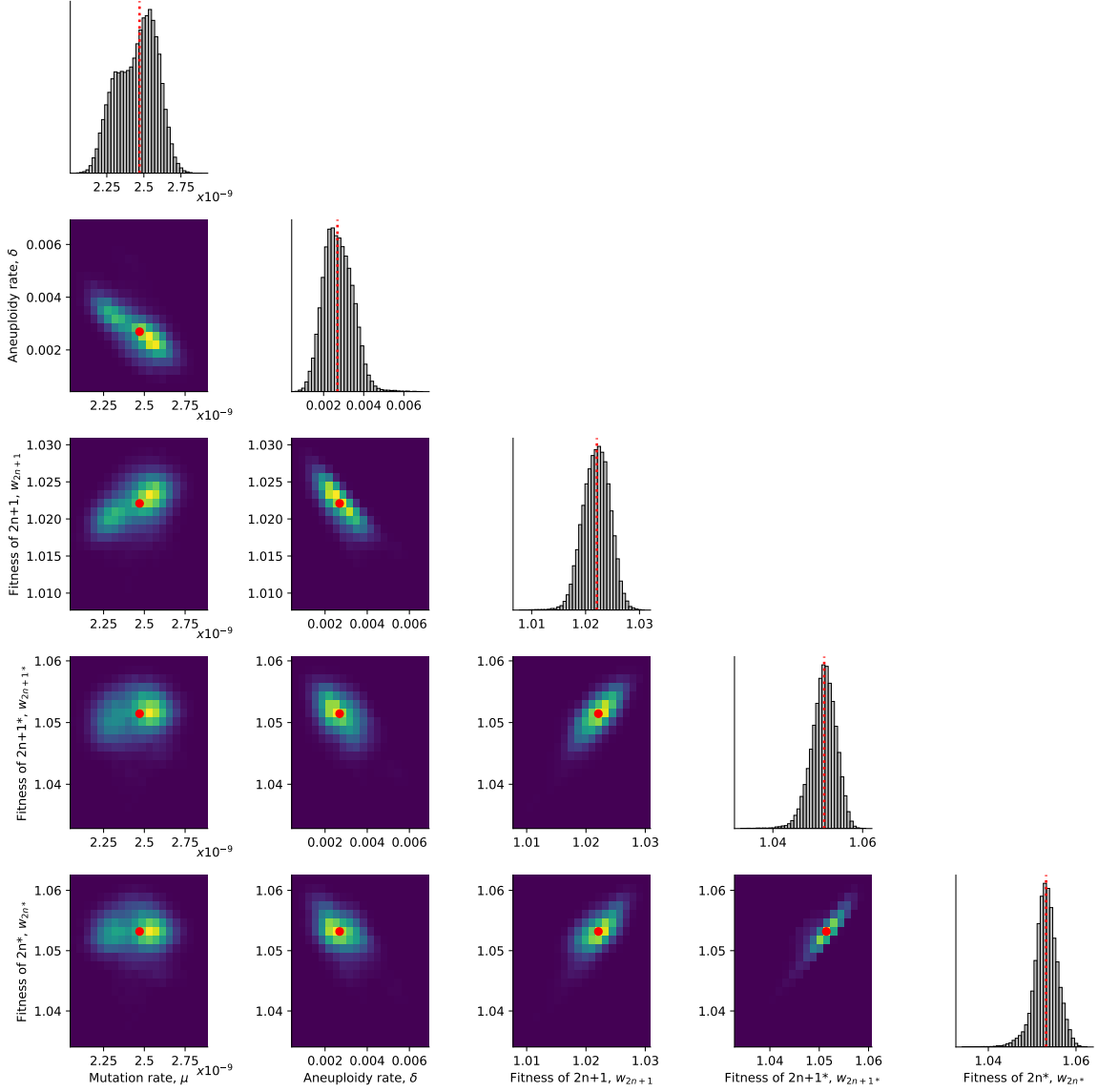


Figure S8: Posterior distribution of parameters inferred with the extended prior distribution. On the diagonal, the inferred posterior distribution of each model parameter. Below the diagonal, the inferred joint posterior distribution of pairs of model parameters (dark purple and bright yellow for low and high density, respectively). Red markers and orange lines for the joint MAP estimate (which may differ from the marginal MAP, as the marginal distribution integrates over all other parameters).

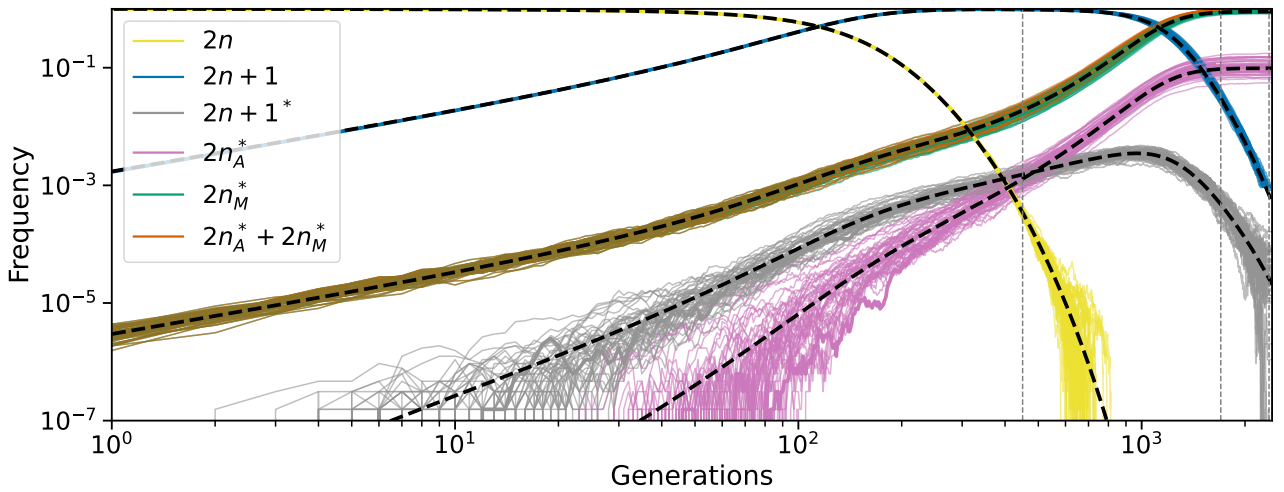


Figure S9: Posterior predicted genotype frequencies in log-log scale. Frequency dynamics of the different genotypes with MAP parameter estimates, same as Figure 4A, but in log-log scale. Black dashed curves for a deterministic model without genetic drift. Clearly, appearance of $2n+1$ and $2n_M^*$ is deterministic. Appearance of $2n+1^*$, and therefore $2n_A^*$, is stochastic, however, the frequency dynamics are deterministic above a frequency of roughly 0.001. Note that the $2n_M^*$ and the $2n_A^* + 2n_M^*$ lines are overlapping for much of their trajectories.

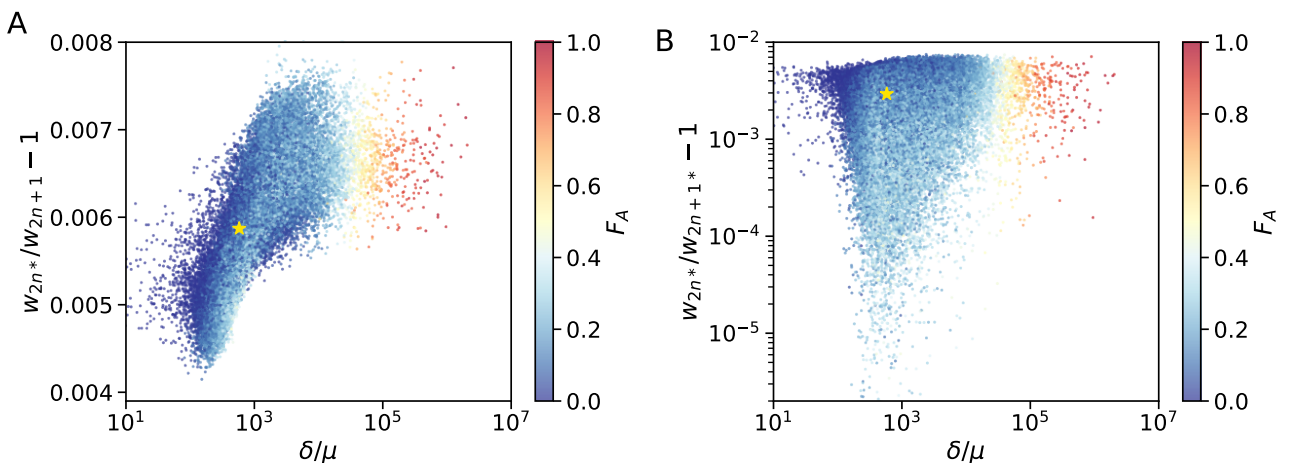


Figure S10: Posterior distribution of F_A . (A,B) F_A values (color coded) as in Figure 4 for different parameter choices on the x- and y-axes. White star denotes the MAP estimate.

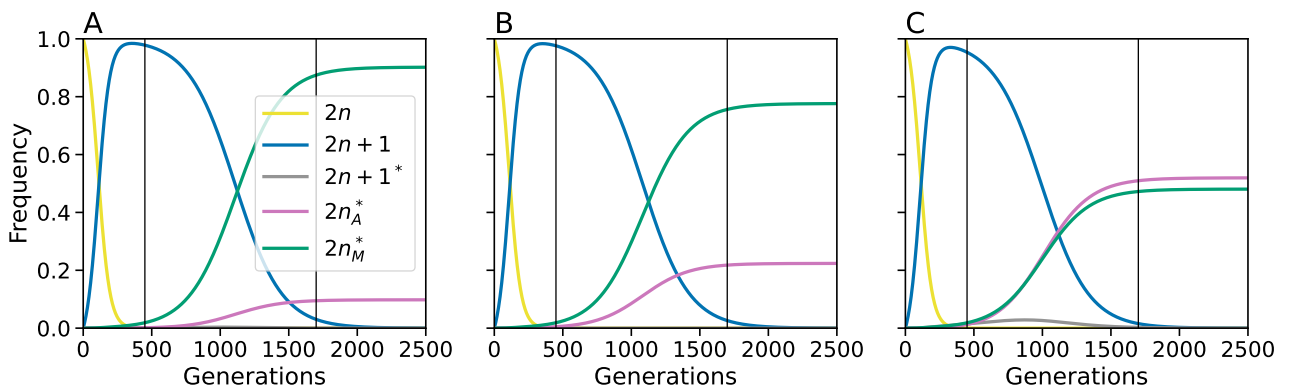


Figure S11: Effect of genomic instability on genotype frequencies. Genotype frequencies in the deterministic model without drift and with MAP parameter estimates (**A**), with 100-fold increase in rate of chromosome loss (transition from $2n + 1^*$ to $2n^*$) (**B**), and with 10-fold increase in mutation rate in aneuploid cells (**C**). Corresponding F_A values are 0.098, 0.223, and 0.519.